

Landsat and Sentinel-derived glacial lake dataset in the China-Pakistan Economic Corridor from 1990 to 2020

Muchu Lesi¹, Yong Nie^{1, *}, Dan H. Shugar², Jida Wang³, Qian Deng^{1, 4}, Huayong Chen¹, Jianrong Fan¹

¹Institute of Mountain Hazards and Environment, Chinese Academy of Sciences, Chengdu, China-

²Water, Sediment, Hazards, and Earth-surface Dynamics (waterSHED) Lab, Department of Geoscience, University of Calgary, Alberta, T2N 1N4, Canada

³Department of Geography and Geospatial Sciences, Kansas State University, Manhattan, Kansas 66506, USA

⁴University of Chinese Academy of Sciences, Beijing 100190, China

*Corresponding author, nieyong@imde.ac.cn

Abstract. The China-Pakistan Economic Corridor (CPEC) is one of the flagship projects of the One Belt One Road Initiative, which faces threats from water shortage and mountain disasters in the high-elevation region, such as glacial lake outburst floods (GLOFs). An up-to-date high-quality glacial lake dataset with parameters such as lake area, volume and type, which is fundamental to water resource and flood risk assessments, and predicting glacier-lake evolutions, is still largely absent for the entire CPEC. This study describes a glacial lake dataset for the CPEC using a threshold-based mapping method associated with rigorous visual inspection workflows. This dataset includes (1) multi-temporal inventories for 1990, 2000, and 2020 produced from 30 m resolution Landsat images, and (2) a glacial lake inventory for the year 2020 at 10 m resolution produced from Sentinel-2 images. The results show that, in 2020, 2234 lakes were derived from the Landsat images, covering a total area of $86.31 \pm 14.98 \text{ km}^2$ with a minimum mapping unit of 5 pixels (4500 m^2), whereas 7560 glacial lakes were derived from the Sentinel-2 images with a total area of $103.70 \pm 8.45 \text{ km}^2$ with a minimum mapping unit of 5 pixels (500 m^2). The discrepancy shows that Sentinel-2 is able to detect a significant quantity of smaller lakes than Landsat due to its finer spatial resolution. Glacial lake data in 2020 was validated by Google Earth-derived lake boundaries with a median (\pm standard deviation) difference of $7.66 \pm 4.96 \%$ for Landsat-derived product and $4.46 \pm 4.62 \%$ for Sentinel-derived product. The total number and area of glacial lakes from consistent 30 m resolution Landsat images remain relatively stable despite a slight increase from 1990 to 2020. A range of critical attributes have been generated in the dataset, including lake types and mapping uncertainty estimated by an improved Hanshaw's equation. This comprehensive glacial lake dataset has potential to be widely applied in studies on water resource assessment, glacial lake-related hazards, glacier-lake interactions, and is freely available at <https://doi.org/10.12380/Glaci.msdc.000001> (Lesi et al., 2022).

1 Introduction

Glaciers in High-mountain Asia (HMA) play a crucial role in regulating climate, supporting ecosystems, modulating the release of freshwater into rivers, and sustaining municipal water supplies (Wang et al., 2019; Viviroli et al., 2020), agricultural irrigation, and hydropower generation (Pritchard, 2019; Nie et al., 2021). Most HMA glaciers are losing mass in the context of climate change (Brun et al., 2017; Maurer et al., 2019; Shean et al., 2020; Bhattacharya et al., 2021), therefore, unsustainable glacier melt and the passing of peak water are reducing the hydrological role of glaciers (Huss and Hock, 2018) and impacting downstream ecosystem services, agriculture, hydropower and other socioeconomic values (Carrivick and Tweed, 2016; Nie et al., 2021). The present and future glacier changes not only impact water supply for downstream area but also alter the frequency and intensity of glacier-related hazards, such as glacier lake outburst floods (GLOFs) (Nie et al., 2018; Rounce et al., 2020; Zheng et al., 2021), and rock and ice avalanches (Shugar et al., 2021). Global glacial lake number and total area both increased between 1990 and 2018 in response to glacier retreat and climate change (Shugar et al., 2020), affecting the allocation of freshwater resource. The Indus is globally the most important and vulnerable water tower unit where glaciers, lakes and reservoir storage contribute about two-thirds of the water supply (Immerzeel et al., 2020). Ice-marginal lakes store $\sim 1\%$ of total ice discharge in Greenland and accelerate lake-terminating ice velocity by $\sim 25\%$ (Carrivick et al., 2022). An increasing

frequency and risk of GLOFs (Nie et al., 2021; Zheng et al., 2021) is threatening Asian population and infrastructures in the mountain ranges, such as the China-Pakistan Economic Corridor (CPEC), as a flagship component of One Belt One Road Initiative (Battamo et al., 2021; Li et al., 2021). The northern section of the CPEC passes through Pamir, Karakoram, Hindu Kush and Himalaya mountains where droughts and glacier-related hazards are frequent and severe (Hewitt, 2014; Bhambri et al., 2019; Pritchard, 2019), threatening local people, the existing, under-construction and planned infrastructures, such as highways, hydropower plants and railways. Understanding the risk posed by water shortage and glacier-related hazards is a critical step to sustainable development for the CPEC.

Glacial lake inventories with a range of attributes benefit water resource assessment and disaster risk assessment related to glacial lake (Wang et al., 2020; Carrivick et al., 2022), and contribute to predicting glacier-lake evolution and cryosphere-hydrosphere interactions under climate change (Nie et al., 2017; Brun et al., 2019; Maurer et al., 2019; Carrivick et al., 2020; Liu et al., 2020). Remote sensing is the most viable way to map glacial lakes and detect their spatio-temporal changes in the high-elevation zones where in situ accessibility is extremely low (Huggel et al., 2002; Quincey et al., 2007). Studies in glacial lake inventories using satellite observations have been heavily conducted at regional scales recently, such as in the Tibetan Plateau (Zhang et al., 2015), the Himalaya (Gardelle et al., 2011; Nie et al., 2017), the HMA (Wang et al., 2020; Chen et al., 2021), the Tien Shan (Wang et al., 2013), the Alaska (Rick et al., 2022), the Greenland (How et al., 2021) and the northern Pakistan (Ashraf et al., 2017). However, the latest glacial lake mapping in 2020 is still absent along the CPEC. Among existing studies, Landsat archival images are the most widely used due to their multi-decadal record of earth surface observations, reasonably high spatial resolution (30 m), and publicly available distribution (Roy et al., 2014). Freely available Sentinel-2 satellite images show a better potential than Landsat in glacial lake mapping and inventories due to their higher spatial resolution (10 m) and a global coverage, but have only been available since late 2015 (Williamson et al., 2018; Paul et al., 2020). Glacial lake inventories using Sentinel-2 images are relatively scarce at regional scales, and studies of the latest glacial lake mapping as well as comparisons of glacial lake dataset derived from Sentinel-2 and Landsat observations are still lacking.

Discrepancies between various glacial lake inventories (Zhang et al., 2015; Shugar et al., 2020; Wang et al., 2020; Chen et al., 2021; How et al., 2021) result from differences in mapping methods, minimum mapping units, definition of glacial lakes, time periods, data sources and other factors. For example, manual vectorization method was widely adopted at the earlier stage for its high accuracy. However, it is time-consuming associated with high labor intensity and is only practical at regional scales (Zhang et al., 2015; Wang et al., 2020). Automated and semi-automated lake mapping methods, such as multi-spectral index classification (Gardelle et al., 2011; Nie et al., 2017; Zhang et al., 2018; How et al., 2021), have been developed to improve the efficiency of glacial lake inventories using optical images, although manual modification is often unavoidable to assure the quality of lake data impacted by cloud cover, mountain shadows, seasonal snow cover and frozen lake surfaces (Sheng et al., 2016; Wang et al., 2017, 2018). Backscatter images from Synthetic Aperture Radar (SAR) (Wangchuk and Bolch, 2020; How et al., 2021) were used to remove the impact of cloud cover for lake mapping. Besides, other approaches such as hydrological sink

107 detection using DEM (How et al., 2021) and land surface temperature-based detection
108 method (Zhao et al., 2020) were also used for lake inventories. Different classification
109 methods impact the results of lake mapping and monitoring. So far, we are lacking a unified
110 standard for the classification system of glacial lakes (Yao et al., 2018). Existing
111 classification systems are generally used for their individual research purposes, mainly based
112 on the relative positions of glacial lakes and glaciers, the supply conditions of glaciers, and
113 the attributes of dams. In addition to different classification standards, the same type of
114 glacial lakes may also have different names given by different scholars. For example, ice-
115 marginal (Carrivick and Quincey, 2014; Carrivick et al., 2020), ice-contact (Carrivick and
116 Tweed, 2013) and proglacial (Nie et al., 2017) lakes all represent glacial lakes sharing the
117 boundary with glaciers. Glacier lakes in currently available datasets have been traditionally
118 categorized by their spatial relationship with upstream glaciers (Gardelle et al., 2011; Wang
119 et al., 2020; Chen et al., 2021), and classification attributes considering the formation
120 mechanism and the properties of dams are rare or incomplete in the CPEC (Yao et al., 2018;
121 Li et al., 2020). Dam type classification of glacial lakes provides a crucial attribute for
122 glacier-lake interactions and risk assessment (Emmer and Cuřín, 2021). Therefore, an up-to-
123 date glacial lake dataset with critical, quality-assured parameters (e.g. lake area, volume and
124 type) is necessary.

125 This study aims to (1) present an up-to-date glacial lake dataset in the CPEC in 2020 using
126 both Landsat 8 and Sentinel-2 images to accurately document its detailed lake distribution;
127 (2) present two historical glacial lake datasets for the CPEC to show extent in 1990 and 2000
128 using consistent 30-m Landsat images to reveal glacial lake changes at three time periods
129 (1990, 2000 and 2020); and (3) generate a range of critical attributes for glacial lake
130 inventories to benefit studies on water resource evaluation, risk assessment of GLOFs, glacier
131 –lake evolution modeling in the HMA.

132 **2 Study area**

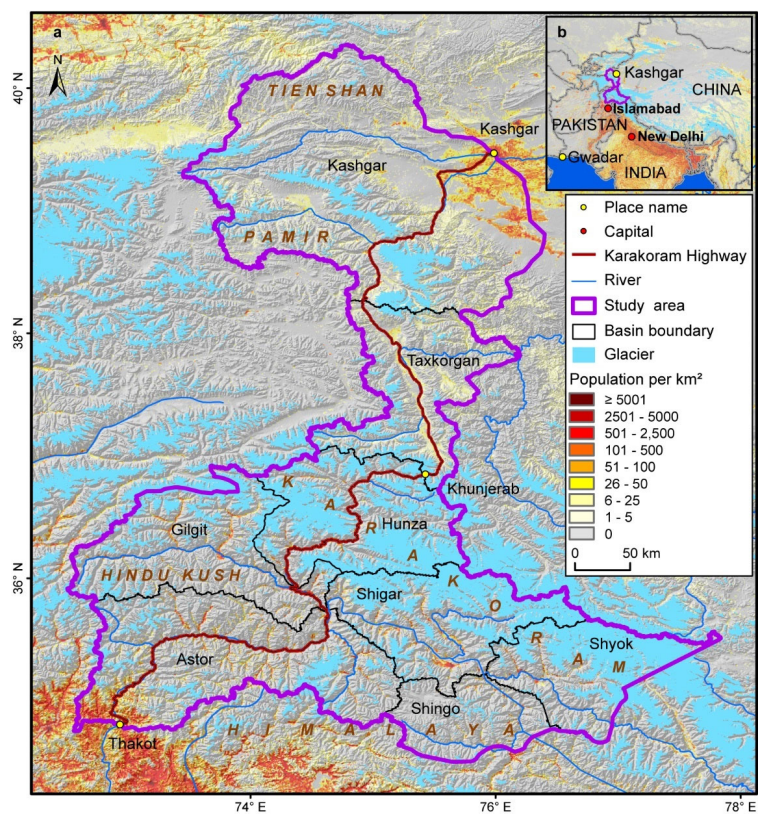


Figure 1. Location of the study area associated with distribution of glaciers (RGI Consortium, 2017), mountains, basins and population (Rose et al., 2021) (a), and its location within the CPCE (b).

The northern part of the CPEC is selected as the study area (Figure 1). The CPCE, originating from Kashgar of the Xinjiang Uygur Autonomous region, China and extending to Gwadar Port, Pakistan (Ullah et al., 2019; Yao et al., 2020), is connecting China and Pakistan via the only Karakoram Highway. The study area covers all the drainage basins along Karakoram Highway starting from Kashgar and ending at Thakot, with a total area of ~125,000 km². The upper Indus basins beyond the Pakistani-administrated border are excluded in this study due to spatial coverage of the CPCE. The entire study area is divided into eight sub-basins, covering most of the Karakoram with the highest elevation up to 8611 m, western Himalaya and Tien Shan, eastern Hindu Kush and Pamir Mountains. The 9710 glaciers in the study area cover a total area of 17,447 km² and nearly 60% of glaciers are distributed in the Karakoram (5818 glaciers with a total area of 14,067.52 km²) (RGI Consortium, 2017). Most glaciers in the western Himalaya and eastern Hindu Kush are losing mass in the context of

带格式的: 字体: 非加粗

climate change (Kääb et al., 2012; Yao et al., 2012; Brun et al., 2017; Shean et al., 2020; Hugonnet et al., 2021), whereas the glaciers in the eastern Karakoram and Pamir have shown unusually little changes, including unchanged, retreated, advanced and surged glaciers (Hewitt, 2005; Kääb et al., 2012; Bolch et al., 2017; Brun et al., 2017; Shean et al., 2020; Nie et al., 2021). The spatially heterogeneous distribution and changes of glaciers are primarily explained as a result of differences in the dominant precipitation-bearing atmospheric circulation patterns that include the winter westerlies the Indian summer monsoon, their changing trends and their interactions with local extreme topography (Yao et al., 2012; Azam et al., 2021; Nie et al., 2021).

3 Data sources

Both Landsat and Sentinel-2 images have been employed to map glacial lakes between 1990 and 2020 in the CPEC (Figure 2). A total number of 71 Landsat Thematic Mapper (TM), Thematic Mapper Plus (ETM+) and Landsat 8 Operational Land Imager (OLI) images with a consistent spatial resolution of 30 m were downloaded from the United States Geological Survey Global Visualization Viewer (GloVis, <https://glovis.usgs.gov/>) to be used to create glacial lake inventories in 1990, 2000 and 2020. High-quality Landsat-5 images around 2010 are insufficient to cover the entire study area, so we were unable to map lakes in 2010 due to Landsat-7's scan-line corrector errors and significant cloud covers. In addition, 39 Sentinel-2 images (23 scenes in 2020) were downloaded from Copernicus Open Access Hub (<https://scihub.copernicus.eu/>) to produce the 10-m resolution glacial lake inventory in 2020. All images used in this study have been orthorectified before download, but we still find that one Sentinel-2 image was not well matched with Landsat images, leading to the discrepancy between the two glacial lake datasets. We manually georeferenced the shifted image to minimize the difference between Sentinel and Landsat derived glacial lakes.

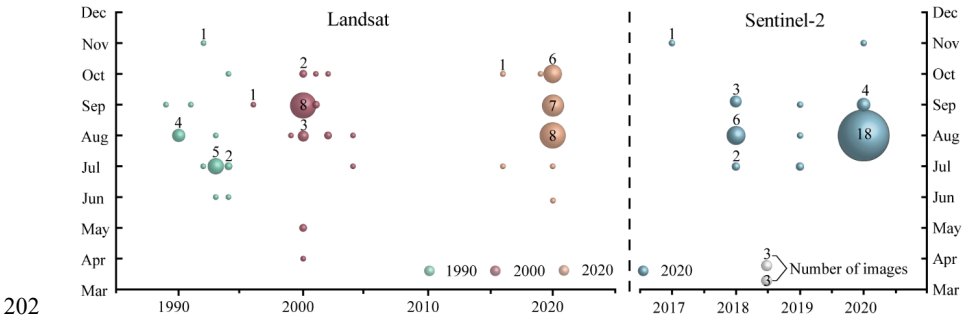
Cloud and snow covers heavily affect the usability of optical satellite images (Wulder et al., 2019) and their availability in the entire study area, so we took advantage of the images acquired before and after each of the baseline years 1990, 2000 and 2020 to construct the glacial lake inventories. Only 4 images in 1990 (the largest covering the study area), 16 images in 2000 and 23 images in 2020 were used for matching baseline year. Spatially, high-quality images in given baseline years were preferentially chosen, or we selected one or more alternative images acquired in adjacent years to delineate glacial lakes by removing the effect of cloud and snow covers. To minimize the impact of intra-annual changes of glacial lakes, most of used images (82% for Sentinel-2 and 75% for Landsat) were acquired from August to October in the given baseline year with cloud coverage of <20% for each image. For some specific scenes where cloud cover exceeded the threshold of 20%, we selected more than one image to remedy the effect of cloud contamination (Nie et al., 2010, 2017; Jiang et al., 2018).

Other datasets used include the Randolph Glacier Inventory version 6.0 (Pfeffer et al., 2014; RGI Consortium, 2017) and the Glacier Area Mapping for Discharge from the Asian Mountains (GAMDAM) glacier inventory (Sakai, 2019). These two glacier datasets were used to determine glacial lake types, such as ice-contact, ice-dammed and unconnected-glacier-fed lakes. The Shuttle Radar Topography Mission Digital Elevation Model (SRTM DEM) at a 1-arc second (30 m) resolution (Jarvis et al., 2008) was employed to extract the altitudinal characteristics of the glacial lakes. The absolute vertical accuracy of the SRTM

带格式的: 字体: (中文) 宋体, 非加粗

DEM is 16 m (90%) (Rabus et al., 2003; Farr et al., 2007). We also applied other published glacial lake datasets for comparative analysis. They include the glacial lake inventories of HMA in 1990 and 2018 downloaded from <http://doi.org/10.12072/casnw.064.2019.db> (Wang et al., 2020), the Third Pole region in 1990, 2000 and 2010 publicly shared at <http://en.tpdatabase.cn/> (Zhang et al., 2015), the Tibet Plateau from 2008 to 2017 accessed at <https://doi.org/10.5281/zenodo.3700282> (Chen et al., 2021), and the entire world in 1990, 2000 and 2015 provided at https://nsidc.org/data/HMA_GLI/versions/1 (Shugar et al., 2020). In addition, field survey data collected between 2017 and 2018 were also used to assist in lake mapping and glacial lake type classification.

201



202

203 **Figure 2.** Acquisition years and months of Landsat and Sentinel-2 images selected for glacial lake
204 inventories. The bubble size indicates the available high-quality image number.

205 4 Glacial lake inventory methods

206 4.1 Definition of glacial lakes

207 We consider a glacial lake as one that formed as a result of modern or ancient glaciation.
208 Contemporary glacial lakes are easily recognized using a combination of glacier inventories
209 and remote sensing images. Ancient glacial lakes can be identified from periglacial
210 geomorphological characteristics, including moraine remnants and U-shaped valleys that are
211 discernible from satellite observations (Post and Mayo, 1971; Westoby et al., 2014; Nie et al.,
212 2018; Martin et al., 2021). A 10-km buffering distance of RGI 6.0 glacier boundaries that has
213 been widely used in previous studies (Zhang et al., 2015; Wang et al., 2020), was created to
214 help mapping glacial lakes. A few glacial lakes in the study area (a total of 84 lakes for
215 Sentinel-2 dataset and 55 lakes for Landsat dataset in 2020) beyond the buffering zone,
216 located near buffering boundaries, were intentionally included due to clear evidence of
217 glaciation (Figure 3). Landslide-dammed lakes (Chen et al., 2017) in the buffering
218 zone were excluded in our inventories because of their irrelevance to glaciation. All glacial
219 lakes in the study area were mapped according to our definition. We were able to implement
220 this definition by carefully leveraging the spectral properties of glacial lakes and the
221 periglacial geomorphological features that are often evident in remote sensing images (see
222 more in sections 4.3 and 4.4).

223

域代码已更改

域代码已更改

带格式的: 字体: 非加粗

域代码已更改

域代码已更改

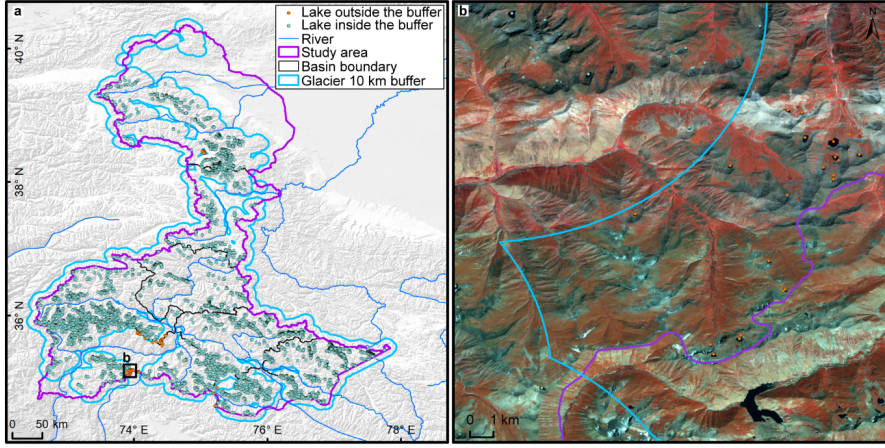


Figure 3. The 10-km buffer zone of RGI 6.0 glacier boundaries (a) and Sentinel-derived glacial lakes located near buffering boundary within the study area (b).

4.2 Interactive lake mapping

A human-interactive and semi-automated lake mapping method (Wang et al., 2014; Nie et al., 2017, 2020) was adopted to accurately extract glacial lake extents using Landsat and Sentinel-2 images, based on the Normalized Difference Water Index (NDWI) (Mcfeeters, 1996). The NDWI uses the green and near infrared bands and is calculated by the following equation:

$$NDWI = \frac{Band_{Green} - Band_{NIR}}{Band_{Green} + Band_{NIR}} \quad (1)$$

where the green band and near infrared band were provided by both Landsat and Sentinel multispectral images.

Specifically, the method calculated the NDWI histogram based on the pixels with each user-defined and manually-drawn region of interest. The NDWI threshold that separates lake surface from land was interactively determined by screening the NDWI histogram against the lake region in the imagery (Wang et al., 2014; Nie et al., 2020). This way, the determined NDWI threshold can be well-tuned to adapt various spectral conditions of the studied glacier lakes. The raster lake extents segmented by the thresholds were then automatically converted to vector polygons. We first completed the glacial lake inventory in 2020 using this interactive mapping method, and the 2020 inventory was then used as a reference to facilitate the lake mapping for other periods.

The minimum mapping unit (MMU) was set to 5 pixels for both Landsat (0.0045 km²) and Sentinel-2 images (0.0005 km²) in this study. MMU determines the total number and area of glacial lakes in the dataset, and varies in the previous studies, such as 3 pixels (Zhang et al., 2015), 6 pixels (Wang et al., 2020), or 9 pixels (Chen et al., 2021) for a regional scale, or 55 pixels (Shugar et al., 2020) for a global scale. While a smaller threshold leads to a large quantity of lakes mapped, it also generates larger mapping noises or uncertainties.

252 Considering this signal-noise balance and our focus on identifying prominent glacier lake
253 dynamics in the study area, we opted to use 5 pixels as the MMU for both Landsat and
254 Sentinel-2 images.

255 Several procedures were taken to assure the quality assurance and quality control for lake
256 mapping, including 1) visual inspection and modification using the threshold-based mapping
257 method for each lake according to Landsat, Sentinel-2 and Google Earth high-resolution
258 images overlaying preliminarily lake boundary extraction at the given time period; 2) time
259 series check for Landsat-derived glacial lake datasets from 1990 and 2020, and cross-check
260 between Landsat and Sentinel-2-derived lake dataset in 2020 to reduce errors of omission and
261 commission; 3) topological validation of glacial lake mapping, such as repeated removal,
262 elimination of small sliver polygons; and 4) logical check for lake types between two
263 classification systems of glacial lakes. False lake extents resulting from cloud or snow cover,
264 lake ice, and topographic shadows (Nie et al., 2017, 2020) were modified using previous
265 semi-automated mapping method based on alternative images acquired in adjacent years.
266 Those procedures were time-consuming, but helped to minimize the effect of cloud and snow
267 covers, lake mapping errors, and to maximize the quality of the produced lake product and
268 the derived glacial lake changes.

269 4.3 Classification of glacial lakes

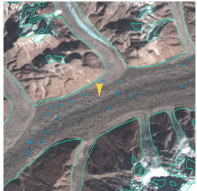


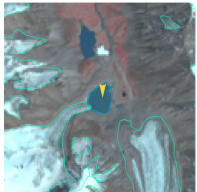
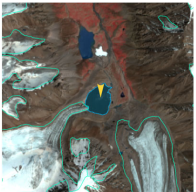
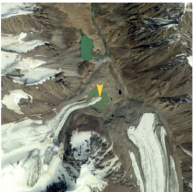
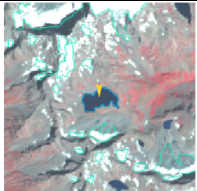
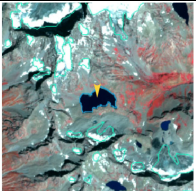
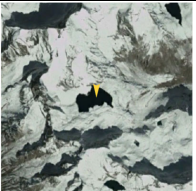
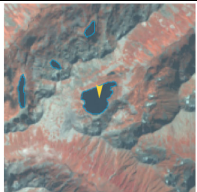
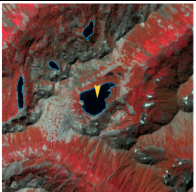
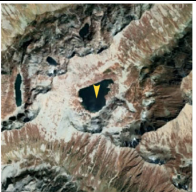
270 Two glacial lake classification systems (GLCS) have been established based on relationship
271 of interaction between glacial lakes and glaciers as well as lake formation mechanism and
272 dam material properties. In the first GLCS (GLCS1), glacial lakes were classified into four
273 types based on their spatial relationship to upstream glaciers: supraglacial, ice-contact,
274 unconnected-glacier-fed lakes, and non-glacier-fed lakes according to Gardelle et al. (2011)
275 and Carrivick et al. (2013). Alternatively, combining the formation mechanism of glacial
276 lakes and the properties of natural dam features, glacial lakes were classified into five
277 categories (herein named GLCS2) modified from Yao's classification system (2018):
278 supraglacial, end-moraine-dammed, lateral-moraine-dammed, glacial-erosion lakes and ice-
279 dammed lakes. Subglacial lakes were excluded due to the mapping challenge from spectral
280 satellite images alone. Characterization and examples for each type are provided in Table
281 1 and Table 2. Individual glacial lakes were categorized to the specific types
282 for each GLCS according to available glacier inventory data, geomorphological and spectral
283 characteristics interpreted from Landsat, Sentinel and Google Earth images. The synergy of
284 these two GLCSs is beneficial to predicting glacier-lake evolutions and providing
285 fundamental data for water resource and glacial lake disaster risk assessment.
286

带格式的: 字体: 非加粗

带格式的: 字体: 非加粗

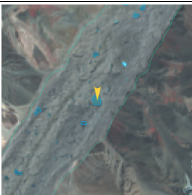

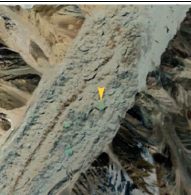
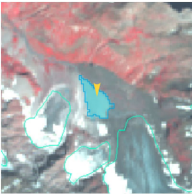
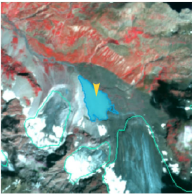


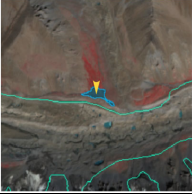
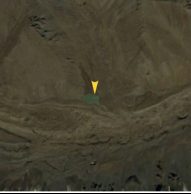

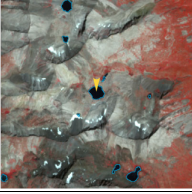


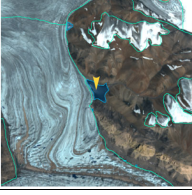
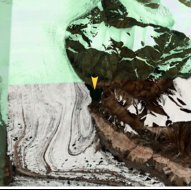
287
p88
289
290

Table 1. Classification system of glacial lake types ([GLCSI](#)) according to the relationship between glacial lakes and glaciers (© Google Earth 2019). Glacier outlines are from RGI 6.0 ([RGI Consortium, 2017](#)), and the yellow marker represents target lake.

Lake types	Characteristics	Landsat	Sentinel-2	Google Earth
Supraglacial	Lakes formed on the surface of glaciers, generally dammed by ice and thin debris. Case location: 35°43'49.74" N 76°13'53.88" E			
Ice-contact	Lakes dammed by moraine, ice or bedrock, supplied by glacial meltwater and shared boundary with glaciers. Case location: 39°09'32.40" N 73°43'12.00" E			
Unconnected-glacier-fed	Lakes currently supplied by upstream glacial meltwater but disconnected with glaciers. Case location: 35°47'60.00" N 72°55'15.60" E			
Non-glacier-fed	Lakes formed by glaciology, dammed by moraine or bed rock, and currently not supplied by glacial meltwater. Case location: 34°50'39.99" N 74°48'29.31" E			

291

Table 2. Classification system of glacial lake types (GLCS2) according to the formation mechanism of glacial lakes and dam material properties (© Google Earth 2019). Glacier outlines from RGI 6.0 (RGI Consortium, 2017), and the yellow marker represents target lake.

Lake types	Characteristics	Landsat	Sentinel-2	Google Earth
Supraglacial	Lakes formed on the surface of glaciers, generally dammed by ice and thin debris. Case location: 36°46'7.39" N 74°20'7.59" E			
End-moraine-dammed	Lakes formed behind moraines as a result of glacier retreat and downwasting. Case location: 35°42'50.40" N 73°09'57.60" E			
Lateral-moraine-dammed	Lakes formed behind lateral glacial moraine ridges and dammed by debris, different from ice-dammed glacial lake. Case location: 38°28'45.62" N 75°20'52.30" E			
Glacial-erosion	Lakes formed in depressions created by glacial over-deepening. Bedrock dam dominates, partially superimposed by top moraine in rugged terrain. Dams are unclear in the satellite images. Case location: 35°55'55.56" N 73°38'20.13" E			
Ice-dammed	Lakes formed behind glaciers, dammed by glacier ices (partially covered by debris on the top). Case location: 35°28'31.32" N 77°30'46.81" E			

4.4 Attributes of glacial lake data

A total of 18 attribute fields were input into our glacial lake datasets (Table 3Table 3). They include lake location (longitude and latitude), lake elevation (centroid elevation), orbital number of the image source, image acquisition date, lake area, lake perimeter, lake types of the two GLCSs, mapping uncertainty, lake water volume and the country, sub-basin, and mountain range associated with the lake. Amongst the attributes, lake location was calculated based on

带格式的: 字体: 非加粗

the centroid of each glacial lake polygon associated with the DEM, N represents northing and E represents easting. Orbital number of the image source was filled with the corresponding satellite image, with the codes expressed as “PxxxRxxx” or “Txxxxx”, where P and R indicate the path and row for Landsat image and T represents the tile of Sentinel-2 image associated with 5 digit code of military grid reference system. SceneID indicated identifying information of image source for Landsat or Sentinel-2, consisted of the orbital number, sensor ID and acquisition date (YYYYMMDD) for Landsat image, or the orbital number and acquisition date (YYYYMMDD) for Sentinel-2 image. Area and perimeter were automatically calculated based on glacial lake extents. Lake water volume was estimated by area-volume empirical equation (Cook and Quincey, 2015). Lake types were attributed using the characterization and interpretation marks described in Section 4.3. Mapping uncertainty was estimated using our modified equation which will be introduced in section 4.5 and appendix tutorial. Located country, sub-basin and mountain range of each glacial lake was identified by overlapping the geographic boundaries of countries, basins and mountain ranges.

Table 3. Attributes of glacial lake dataset.

Field Name	Type	Description	Note
FID or OBJECTID	Object ID	Unique code of glacial lake	Number
Shape	Geometry	Feature type of glacial lake	Polygon
Latitude	String	Latitude of the centroid of glacial lake polygon	Degree minute second
Longitude	String	Longitude of the centroid of glacial lake polygon	Degree minute second
Elevation	Double	Elevation of the centroid of glacial lake polygon	Unit: meter above sea level
SceneIDIMGSOURCE	String	Scene ID of image source for Landsat or Sentinel-2 Path and row numbers for Landsat image based on World Reference System 2 or Tile number for Sentinel image based on military grid reference system	PxxxRxxx_xxxDYYYYMMDD or Txxxxx_YYYYMMDD
ACQDATE	String	Acquisition date of source	YYYYMMDD

带格式的: 字体颜色: 红色

带格式的: 字体颜色: 红色

Field Name	Type	Description	Note
		image	
GLCS1	String	The first classification system of glacial lakes based on relationship of interaction between glacial lakes and glaciers	Supraglacial, Ice-contact, Unconnected-glacier-fed, None-glacier-fed
GLCS2	String	The second classification system of glacial lakes based on lake formation mechanism and dam material properties	Supraglacial, End-moraine-dammed, Lateral-moraine-dammed, Glacial-erosion and Ice-dammed
Basin	String	Basin name where glacial lake locates in	
Mountain	String	Mountain name where glacial lake locates in	
Country	String	Country name where glacial lake locates in	
Perimeter	Double	Perimeter of glacial lake boundary	Unit: meter
Area	Double	Area of glacial lake coverage	Unit: square meter
<u>AreaUncertainty</u>	Double	<u>Area u</u> ncertainty of glacial lake mapping estimated based on modified Hanshaw's equation (2014)	Unit: square meter
<u>Volume</u>	Double	<u>Water volume of glacial lake</u> estimated by area-volume-empirical equation	<u>Unit: square meter</u>
Operator	String	Operator of glacial lake dataset	Muchu, Lesi

带格式的: 字体颜色: 深红

Field Name	Type	Description	Note
Examiner	String	Examiner of glacial lake dataset	Yong, Nie
Volume	Double	Water volume of glacial lake estimated by area-volume empirical equation	Unit: cubic meter

带格式的: 字体颜色: 文字 1

带格式的: 字体颜色: 文字 1

带格式的: 字体颜色: 文字 1

带格式的: 字体颜色: 文字 1

318

319 4.5 Error and uncertainty assessment

320 4.5.1 Improved uncertainty estimating method

321 We modified Hanshaw's (2014) equation that had been used to calculate lake-area mapping
 322 uncertainty. Lake perimeter and displacement error are widely used to estimate the
 323 uncertainty of glacier and lake mapping from satellite observation (Carrivick and Quincey,
 324 2014; Hanshaw and Bookhagen, 2014; Wang et al., 2020). Hanshaw and Bookhagen (2014)
 325 proposed an equation to calculate the error of area measurement by the number of edge pixels
 326 of the lake boundary multiplied by half of a single pixel area. The number of edge pixels is
 327 simply calculated by the perimeter divided by the grid size. The equation is expressed as
 328 below:

$$329 \quad Error(1\sigma) = \frac{P}{G} \times 0.6872 \times \frac{G^2}{2} \quad (2)$$

$$330 \quad D = \frac{Error(1\sigma)}{A} \times 100\% \quad (3)$$

331 Where G is the cell size of the remote sensing imagery (10 m for Sentinel-2 image and 30 m
 332 for Landsat image). P is the perimeter of individual glacial lake (m), and the coefficient of
 333 0.6872 (1σ), which means nearly 69% of the edge pixels are subject to errors (Hanshaw and
 334 Bookhagen, 2014), was chosen assuming that area measurement errors follow a Gaussian
 335 distribution. Relative error (D) was calculated by equation 3, in which A is the area of an
 336 individual glacial lake.

337 In the original equation 2, the number of edge pixels varies by the shape of lake and is
 338 indicated by $\frac{P}{G}$. However, the pixels in the corner are double counted (Figure 4Figure 4). The
 339 total number of repeatedly calculated edge pixels equals the number of inner nodes.
 340 Therefore, we adjusted the calculation of the actual number of edge pixels as the maximum of
 341 edge pixels ($\frac{P}{G}$) subtracting the number of inner nodes. Accordingly, the equation of
 342 uncertainty estimation for lake mapping is modified as below:

$$343 \quad Error(1\sigma) = (\frac{P}{G} - N_{Inner}) \times 0.6872 \times \frac{G^2}{2} \quad (4)$$

344 Where N_{Inner} is the number of inner nodes (inflection points) of each lake. The modified

带格式的: 字体: 非加粗

equation is also suitable for lakes with islands (as illustrated in Figure 4b).

For polygons without islands (Figure 4a), use the following equation:

$$N_{Inner} = \left(\frac{N_{Total} - 4 - 1}{2} \right) \quad (5)$$

N_{Total} is the total number of nodes, including both the outer and inner. N_{Total} is calculated by the “Field Calculator” in ArcGIS, in some cases, it is necessary to remove the redundant nodes before calculating the total number of nodes (See the Appendix for more details). An inner node is a polygon vertex where the interior angle surrounding it is greater than 180 degrees. An outer node is the opposite of the inner node, where the interior angle is less than 180 degrees. We found that the outer nodes are usually four more than the inner nodes in our glacial lake dataset. The total nodes in ArcGIS contain one overlapping node to close the polygon, meaning the endpoint is also the startpoint. This extra count was deleted in the calculation (equation 5).

For polygons with island (Figure 4b) use the following equation:

$$N_{Inner} = \left(\frac{N_{Total} - (N_{Island} + 1) \times 5}{2} \right) \quad (6)$$

N_{Island} is the number of islands within each polygon. A calculation method of N_{Island} is given in the Appendix.

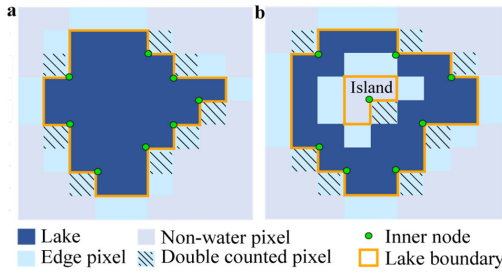


Figure 4. Sketch of estimating the actual edge pixels for uncertainty calculation of individual glacial lake (with (a) and without islands (b)).

4.5.2 Validation of glacial lake mapping

A total of 89 glacial lakes were selected by stratified random sampling and manually digitized based on the Google Earth ~~high-resolution~~ images in circa 2020 with a spatial resolution of ~2 m acquired from WorldView, GeoEye, Pleiades etc. satellites to further validate the absolute error of ~~the our~~ glacial lake ~~mapping products~~ in 2020 due to lacking of field measurements for glacial lakes in the study area. During the sampling, we set a ~~regulation of~~ minimum lake area ~~greater than to be~~ 4500 m² and a relative ~~differing difference~~ between Landsat- and Sentinel-derived lake areas less than 18% (nearly equaling to the average relative error of ±17.36% for Landsat lake mapping) in order to minimize the effect of lake changes from multi-temporal satellite observations in circa 2020. The 89 sample lakes range from 0.005 km² to 0.802 km² with a median (standard deviation) size of 0.047±0.134 km²

377 and a total area of 8.033 km² for Landsat-derived dataset, ~~whereas and ranging range~~ from
378 0.005 km² to 0.849 km² with a median (standard deviation) size of 0.045±0.144 km² and a
379 total area of 8.447 km² for Sentinel-derived dataset.
380

381 **5 Results**

382 5.1 Glacier lake distribution and changes observed from Landsat

383 We mapped 2,234 glacial lakes for 2020 across the studied CPEC from Landsat-8 images,
384 with a total area of 86.31±14.98 km² (~~Figure 5~~Figure 5a and b). Unconnected-glacier-fed
385 lakes are dominant in the first classification system, followed by non-glacier-fed lakes
386 (~~Figure 6~~Figure 6) whereas glacial-erosion lakes dominate at both number (1478) and area
387 (57.02 km²) in the second classification system (~~Figure 7~~Figure 7), followed by end-moraine-
388 dammed lakes and supraglacial lakes. Among the classified lakes, 137 are ice-contact lakes
389 and cover an area of 5.56 km², implying a higher mean size of ice-contact lakes than
390 supraglacial lakes.
391

带格式的: 字体: 非加粗

带格式的: 字体: 非加粗

带格式的: 字体: 12 磅, 非加粗

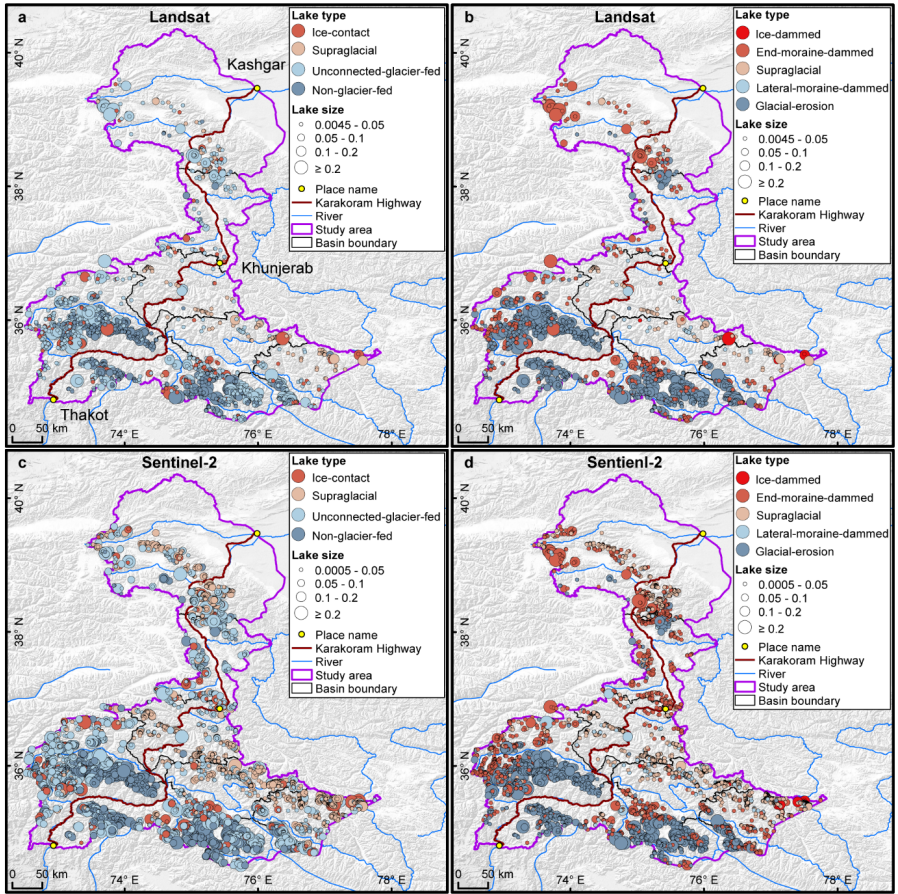


Figure 5. Distribution of glacial lakes in 2020 extracted from Landsat (a, b) and Sentinel-2 (c, d) images. Panels a and c are classified by GLCS1, and GLCS2 for sub-graph b and d.

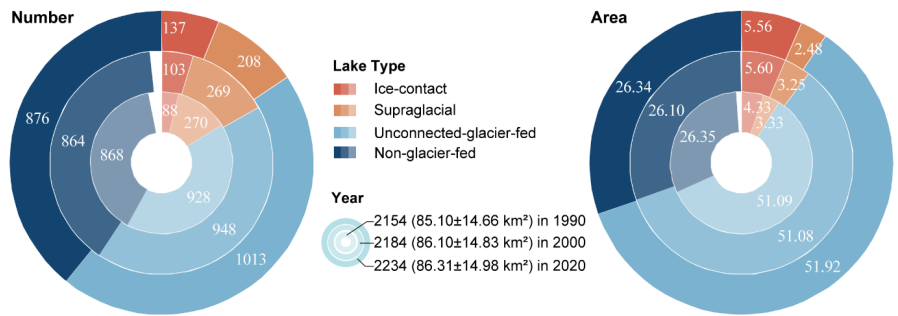


Figure 6. Number and area of different types of glacial lakes classified based on the condition of glacier

supply in the study area (GLCS 1). The outermost ring represents glacial lake data in 2020, middle ring for 2000 and innermost ring for 1990. Lake number and area in 2020 were selected as reference, meaning a concept of "100 %" for a complete ring. Labeled values are scaled in degrees rather the radius of rings.

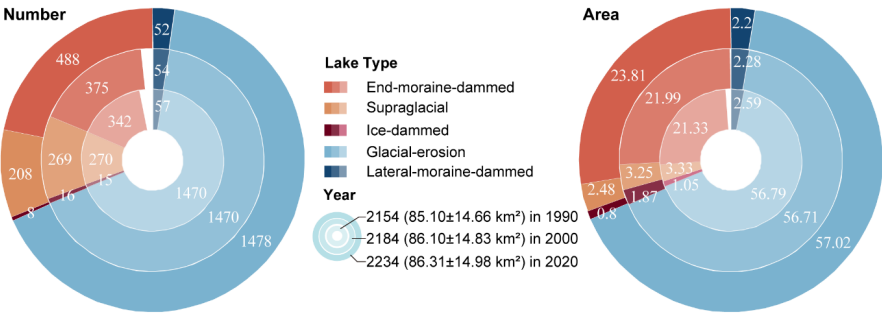


Figure 7. Number and area of different types of glacial lakes classified based on glaciation and nature of dam in the study area (GLCS 2). The outermost ring represents glacial lake data in 2020, middle ring for 2000 and innermost ring for 1990. Lake number and area in 2020 were selected as reference, meaning a concept of "100 %" for a complete ring. Labeled values are scaled in degrees rather the radius of rings.

The total number and area of glacial lakes in the study remain relatively stable with a slight increase between 1990 and 2020, and the changes in count and area among various types of glacial lakes vary substantially (Figure 6Figure 6 and Figure 7Figure 7). From 1990 to 2020, the total number of glacial lakes increased by 80 or 3.70%, while the area grew by 1.21 km² (or 1.42%). In GLCS1, unconnected-glacier-fed lakes have the largest increase in number, followed by ice-contact and non-glacier-fed lakes, whereas supraglacial lakes decreased by 62 in count. Ice-contact lakes expanded by 1.24 km² (equaling an increase of 26% in ice-contact lakes), contributed one third of the total area increase. Supraglacial lakes decreased by 0.85 km² in area whereas the areas of unconnected-glacier-fed and non-glacier-fed lakes remained stable as a result of disconnections from glaciers (Figure 6Figure 6). In GLCS2, end-moraine-dammed lakes increased by 2.48 km² and contributed most of the glacier lake area expansion, whereas supraglacial, ice-dammed and lateral-moraine-dammed lakes decreased slightly in both number and area. Glacial-erosion lakes accounted for the maximum percentage (about 66% for both count and area) in each time period and remained stable (Figure 7Figure 7).

5.2 Glacier lake distribution observed from Sentinel-2

Sentinel-derived results shows that there are 7,560 glacial lakes (103.70±8.45 km²) in 2020 across the entire CPEC (Table 4Table 4) under a MMU of 5 pixels (500 m²). Compared with Landsat-derived product, glacial lakes from Sentinel-2 have similar spatial distribution characteristics (Figure 5Figure 5); meanwhile, a larger quantity of glacier lakes, with more accurate boundaries and a greater total lake area, were generated from Sentinel-2 images. The smallest size class (0.0005-0.0045 km²) contains the maximum lake number (4,969) but the least lake area (7.73±2.62 km²) (Table 4Table 4), which is not available in the Landsat-

derived lake data due to a coarser spatial resolution. In each size class, there are also a higher number of larger glacial lakes from Sentinel than that from Landsat images. The discrepancy is mainly attributed to the inconsistency of spatial resolutions and image acquisition dates.

Table 4. Count and area of glacial lakes mapped from Sentinel-2 and Landsat images in 2020 between various size classes.

Lake size km ²	Glacial lakes from Sentinel-2 count (km ²)	Glacial lakes from Landsat count (km ²)	Overlap % (%)
0.0005-0.0045	4969 (7.73±2.62)	—	—
0.0045-0.05	2182 (35.52±3.72)	1870 (31.47±9.57)	85.70 (88.60)
0.05-0.1	237 (16.37±0.89)	204 (14.07±2.18)	86.08 (85.95)
0.1-0.2	122 (16.88±0.68)	115 (15.91±1.83)	94.26 (94.25)
≥0.2	50 (27.20±0.54)	45 (24.86±1.40)	90.00 (91.40)
Total	7560 (103.70±8.45)	2234 (86.31±14.98)	—

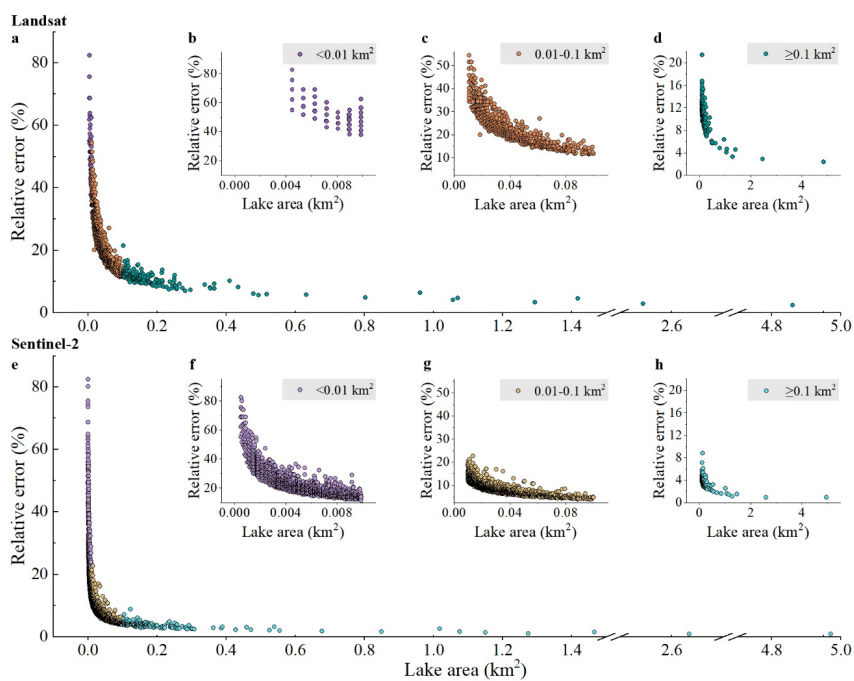
Note: Overlap % (%) represent the rates in count and area calculated by dividing Landsat-derived lake data by Sentinel-derived data in the same size class respectively.

6 Discussions

6.1 Uncertainty and Error and uncertainty of lake mapping

The uncertainty estimated from our improved equation shows that the relative error of individual glacial lake decreases when lake size increases or cell size of remote sensing images reduces (Lyons et al., 2013; Carrivick and Quincey, 2014) (Figure 8). Total area errors of glacial lakes in study area ~~is~~ are approximate ±14.98 km² and ±8.45 km² in 2020 for Landsat and Sentinel-2 dataset, respectively, and the average relative errors ~~is~~ are ±17.36% and ±8.15%. Generally, small lakes have greater relative errors. For example, the mean relative error is 35.38% for Landsat derived glacial lakes between 0.0045 and 0.1 km² and 10.63% for glacial lakes greater than 0.1 km². The mean area error of Sentinel-derived glacial lakes is almost one third of that extracted from Landsat images for glacial lakes of all or specific size groups. Because the relative error was estimated as a function of satellite image spatial resolution and lake perimeter, the calculated error for large lake is proportionally smaller than that of small lake (Salerno et al., 2012) and the error for Landsat-derived lake is naturally greater than that of Sentinel-derived lake at the same size group.

带格式的: 字体: 非加粗



带格式的: 居中

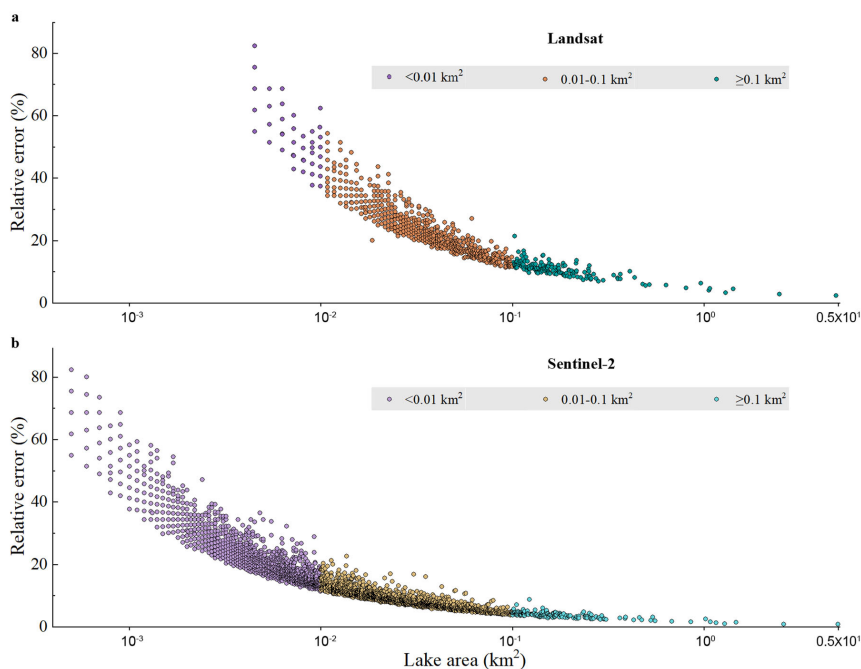


Figure 8. Estimated relative error for glacial lakes of all or specific size ranges in study area. Error estimation is based on the modified equation and lake data extracted from Landsat (a-d) and Sentinel-2 images (be-h).

Our Landsat- and Sentinel-derived glacial lake dataset match well lake boundaries in Google Earth higher resolution images (Figure 9). The mean difference in area is 0.005 km² between Landsat and Google Earth derived lakes and 0.001 km² between Sentinel-2 and Google Earth derived lakes, and major validation samples (84/89) are within the confidence interval of 95%. A dense cluster of validation samples along the 1:1 line indicates a high accuracy in lake mapping (Figure 9c and d). The error of 89 sample lakes is 5.48% in total area between Landsat- and Google Earth-derived data, whereas 0.61% for Sentinel- and Google Earth-derived data. The median (\pm standard deviation) in discrepancy of individual lake area is 7.66 \pm 4.96 % for Landsat- and Google Earth-derived data, whereas 4.46 \pm 4.62 % for Sentinel- and Google Earth-derived data. Our glacial lake dataset shows a satisfactory mapping accuracy, and of which although Sentinel-derived lake data performs more accurate than those from Landsat images. We also validated the sampling Landsat-derived 89 lakes by the existing Landsat-extracted lake data produced by Wang et al. (2020). A total of 83 lakes are available in Wang's data with a mean difference of 0.005 km² in lake area (Figure A8). This also shows an improvement of our lake product in contrast to the existing dataset.

带格式的: 与下段不同页

带格式的: 字体: 非加粗

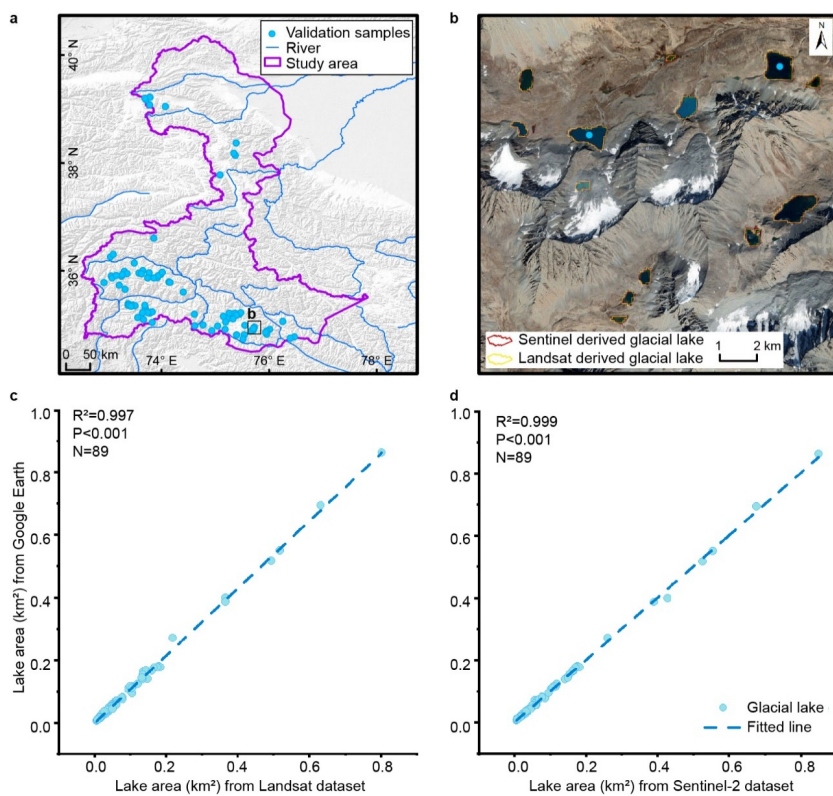
带格式的: 字体: 非加粗

带格式的: 上标

带格式的: 上标

带格式的: 字体: 非加粗

带格式的: 字体: (中文) 宋体



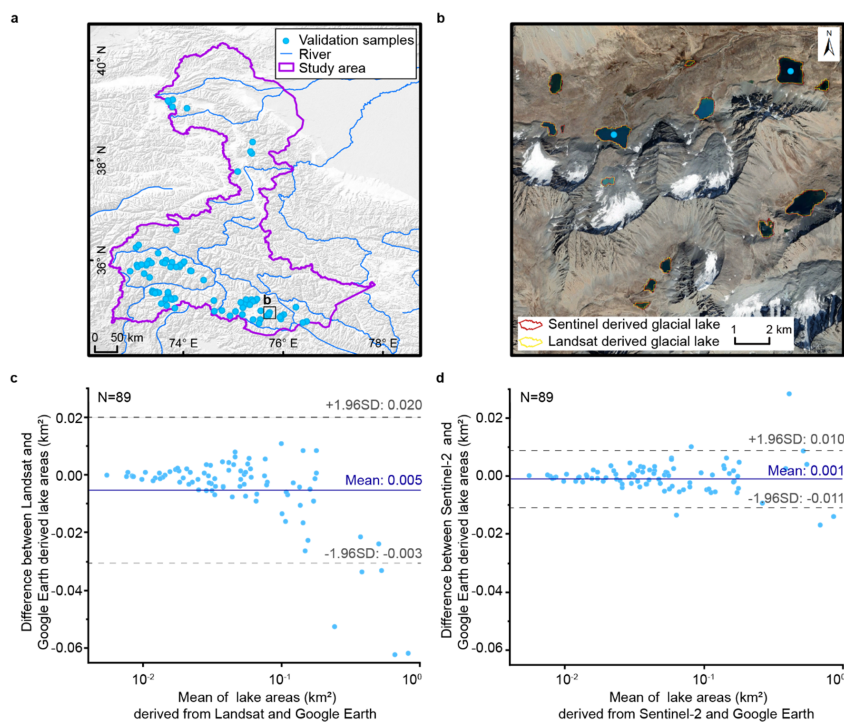


Figure 9. Distribution of validation samples (a), comparison of glacial lakes derived from Landsat and Sentinel-2 overlaying Google Earth image (© Google Earth 2019) in a zoomed site (b), and glacial lake product validated by Google Earth derived lake boundaries (c and d).

6.2 Comparison of Sentinel-2 and Landsat derived products

Glacial lakes from Landsat and Sentinel-2 images have a high consistency in number and area with overlap rates from approximately 86% to 94% for all lakes greater than 0.0045 km² (Table 4 Table 4), indicating a good potential for coordinated utility with Landsat archived observation (Figure 10 Figure 10). Lake extents extracted from Landsat and Sentinel images match well for various types and sizes (Figure 10 Figure 10 and Figure 11 Figure 11, Table 4 Table 4). The best consistency rate reaches 94% for the glacial lakes between 0.1 km² and 0.2 km². The difference in area of glacial lakes extracted from Landsat and Sentinel-2 images generally lies within the uncertainty ranges.

带格式的: 字体: 非加粗

带格式的: 字体: 非加粗

带格式的: 字体: 非加粗

带格式的: 字体: 非加粗

带格式的: 字体: 非加粗

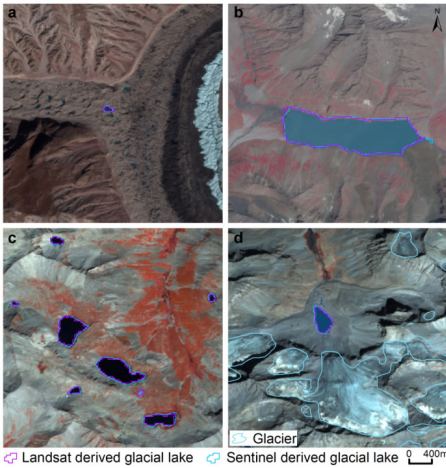


Figure 10. High consistency of lake extents extracted from Landsat and Sentinel-2 images. Lake types shown include supraglacial (a), glacier-fed moraine-dammed (b), unconnected glacial-erosion lake without glacier melt supply (c) and glacier-fed moraine-dammed lakes (d).

Spatial resolution of satellite images plays a primary role in the discrepancies in count and area of glacial lakes extracted from Landsat (30 m) and Sentinel-2 (10 m) observations. Due to a finer spatial resolution, Sentinel-2 images can extract more glacial lakes and more accurate extents than those from Landsat images. We set the same 5 pixels as the MMU for both Landsat and Sentinel-2 images, which corresponds to a minimum area of 0.0045 km² and 0.0005 km², respectively. The minimum mapping area results in generating nearly 5000 more lakes from Sentinel-2 images than from Landsat images, causing the greatest discrepancy in number (Table 4), such as Figure 11a. Small lakes such as supraglacial lakes play an important role in analyzing glacier evolution and supraglacial drainage systems (Liu and Mayer, 2015; Miles et al., 2018), implying a potential of our dataset to be applied in studies of glacier-lake evolutions. Meanwhile, Sentinel-2 images are able to depict boundaries of glacial lake with a lower uncertainty, as for some small islands and narrow channels (Figure 11b and c) were mapped from Sentinel-2 imagery that were unable to be detected in Landsat imagery.

Different acquisition dates between Sentinel-2 and Landsat images also contribute to the discrepancy of those two glacial lake data. Acquiring same-day images from the two sensors were not always possible due to the impacts of cloud contaminations, topographic shadows, snow cover and revisit periods (Williamson et al., 2018; Paul et al., 2020). Glacial lakes are changing temporally in the context of climate and glacier changes. The example is given to supraglacial lakes which showed considerable changes during a short period of time between the applied Landsat and Sentinel-2 images, taking supraglacial lakes for example that evolve dramatically in a short period observed between Landsat and Sentinel-2 images (Figure 11d). Despite our efforts of leveraging all available high-quality images, the overlap of acquisition dates between Landsat and Sentinel-2 images for the same location is relatively

带格式的: 字体: 非加粗

带格式的: 字体: (中文) Times New Roman, 非加粗

带格式的: 字体: (中文) Times New Roman, 非加粗

带格式的: 字体: (中文) Times New Roman, 非加粗

low (only 7 scenes of Sentinel-2 images or 112 glacial lakes in 2020) in this study area, and the consequential temporal gaps led to a difference in the number and area of the derived glacial lakes.

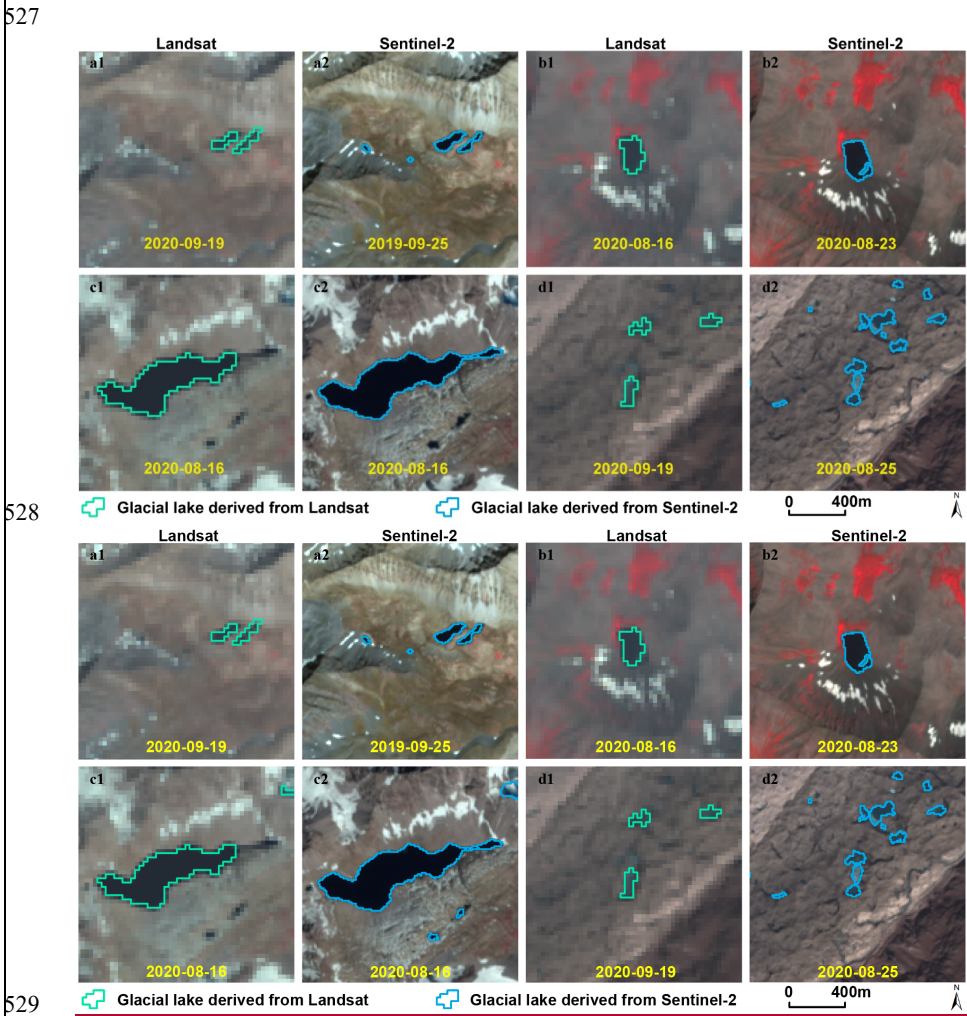


Figure 11. Discrepancy of lake extents extracted from Landsat and Sentinel-2 images.

6.3 Comparison with previous similar dataset

An increasing number of glacier lake datasets have been released over the past years, and most of them were produced from long-term Landsat archives. Regional glacial lake datasets using Sentinel images are scarce. Lack of Sentinel-derived glacial lake data in the study area makes it impossible to compare. Here we selected four available glacial lake datasets to

compare with our Landsat-derived dataset.

We provide the latest glacial lake dataset (in 2020) and the most long-term 30-m Landsat observation (1990 to 2020) for this study, with a range of critical attributes including two types of classification systems. Within the same study area, our 2020 glacial lakes appear to be closest to the 2018 dataset produced by Wang et al. (2020), with the highest overlap of greater than 74.85% in both number and area (Table 5). In Wang et al. (2020), the minimum mapping unit is 6 pixels so their dataset has a smaller lake quantity. However, their dataset contains many large landslide-dammed lakes that are excluded in our glacial lake mapping. As a result, their total glacier lake area is greater than ours. The overlapping rates between Wang's glacial lakes (2020) in 1990 and ours are more than 76.69% in both number and area. However, their results show a distinct increase of glacial lakes in number and area between 1990 and 2018 (Wang et al., 2020) whereas our data show a more stable change between 1990 and 2020. One possible reason is that manually delineating glacial lakes twice by different operators during Wang's lake mapping (2020) exacerbates the errors of mapping. Another reason is that their data contains landslide-dammed lakes that fluctuate greatly with time and expanded recently. One example is the Attabad Lake (Located at 36°18'22.33"N, 74°49'34.36"E).

Table 5. Comparison of different glacial lake datasets sourced from Landsat images in the study area.

Baseline year (period)	Method	MMU m ² (pixels)	Count (km ²)	Other's <u>area</u> / ours— %—(%)	Reference
1990 (1988-1993)	Manual	5400 (6)	1720 (89.68±13.69)	105.8669-17- (76.33)	Wang et al., 2020
1990 (1990-1999)	Automated	50000 (55)	145 (20.28)	36.986-27- (21.66)	Shugar et al., 2020
1990 (1989-1992)	Manual	2700 (3)	622 (51.93±10.15)	61.0227-72- (39.94)	Zhang et al., 2015
1990 (1989-1994)	Semi-automated	4500 (5)	2154 (85.10±14.66)	—	This study
2000 (1999-2001)	Manual	2700 (3)	724 (61.41±11.91)	71.3231-91- (46.97)	Zhang et al., 2015
2000 (2000-2004)	Automated	50000 (55)	155 (22.35)	40.276-78- (23.72)	Shugar et al., 2020
2008	Automated & Manual	8100 (9)	1067 (65.45)	78.0844-14- (53.58)	Chen et al., 2021
2000 (1996-2004)	Semi-automated	4500 (5)	2184 (86.10±14.83)	—	This study
2015 (2015-2018)	Automated	50000 (55)	148 (21.45)	38.776-27- (22.97)	Shugar et al., 2020
2017	Automated & Manual	8100 (9)	1063 (63.23)	75.4745-21- (57.78)	Chen et al., 2021
2018 (2017-2018)	Manual	5400 (6)	1956 (102.46±15.48)	119.2474-57- (85.63)	Wang et al., 2020
2020 (2016-2020)	Semi-automated	4500 (5)	2234 (86.31±14.98)	—	This study

Note: MMU represents minimum mapping units. The % (9%) represent the rates in area calculated by dividing individual glacial

域代码已更改
带格式的: 字体: 非加粗

带格式的: 字体: 9 磅

带格式的: 字体: 9 磅

带格式的: 字体: 9 磅

带格式的: 字体: 9 磅

带格式的: 字体: 9 磅

带格式的: 字体: 9 磅

带格式的: 字体: 9 磅

带格式的: 字体: 9 磅

带格式的: 字体: 9 磅

lake dataset by our Landsat-derived data [greater than the same minimum lake size](#) in the nearest baseline year respectively.

The second highest overlapping rate is approximate 54% for 2008 and 58% for 2017 in area comparing with Chen's data ([Chen et al., 2021](#)). ~~However, the overlapping rate in number is nearly 45% due to their larger minimum mapping unit (9 pixels).~~ Similarly, a minimum mapping unit of 55 pixels (50000 m²) in Shugar et al.'s, dataset ([2020](#)) led to the lowest overlap with less than 24% in area. The dataset from Zhang et al. ([2015](#)) shows fewer glacial lakes in 1990 and 2000 even with a smaller MMU of 3 pixels. By inspecting their dataset, we attributed this anomalous discrepancy to a range of glacial lakes that were missing due to lack of thorough cross-check quality assurance during their manual delineation. Our Landsat derived glacial lake dataset has been visually cross-checked over three time periods after the step of threshold-based semi-automated lake mapping, and also been visually validated by Sentinel-2 derived glacial lakes. Through this series of quality assurance, we aim at delivering one of the most reliable multi-decadal glacial lake products for this study area.

Other factors, such as image quality and acquisition dates, mapping methods and quality assurance workflow, might also lead to the discrepancies between the glacial lake datasets. Despite such discrepancies, an increasing number of publically-shared datasets benefit potential users to select the most suitable one for their objectives. Herein, we provide an up-to-date glacial lake dataset derived from both Landsat and Sentinel-2 observations, which further increased the availability of glacial lake dataset for water resource and GLOFs risk assessment, predicting glacier-lake evolutions ([Carrivick et al., 2020](#)) in the context of climate change.

6.4.3 Limitation and updating plan

We would like to acknowledge several limitations of our glacier lake dataset, largely due the availability of high quality satellite images in the study area and inadequate field survey data ([Wang et al., 2020](#); [Chen et al., 2021](#)). First, it is unlikely to collect enough good-quality images within one calendar year for the entire study area due to high possibility of cloud or snow covers. Even though the capacity of repeat observations for Landsat-8 OLI and Sentinel-2 increased ([Roy et al., 2014](#); [Williamson et al., 2018](#); [Wulder et al., 2019](#); [Paul et al., 2020](#)), the 2020 glacial lake dataset has to employ images acquired in adjacent years besides 2020. Most images used from Landsat and Sentinel-2 platforms were imaged in autumn, and some images taken between April and July and in November also were employed. Distribution and changes in glacial lakes primarily represent the characteristics between August and October. Glacial lakes evolve with time and space ([Nie et al., 2017](#)), and subtle inter- and intra-annual changes ([Liu et al., 2020](#)) for each time period were ignored. Second, field investigation data are limited due to low accessibility of high mountain environment in the study area, which restrained the accuracy in classifying the glacial lake types. Although very high-resolution Google Earth images were utilized to assist in lake type interpretation, occasional misclassification was unavoidable. We implemented two types of classification systems based on a careful utilization of glacier data, DEM, geomorphological features and expert knowledge. However, the lack of in situ survey prohibited a thorough validation of the glacial lake types. Third, the rigorous quality assurance and cross check after semi-automated lake mapping assure the quality of our lake dataset but are still time and cost

prohibitive. State-of-the-art mapping methods, such as deep learning method (Wu et al., 2020), Google Earth Engine cloud-computing (Chen et al., 2021) and synergy of SAR and optical images (Wangchuk and Bolch, 2020; How et al., 2021), would be used in the future to balance product accuracy and time cost.

The glacial lake dataset will be updated using newly collected Landsat and Sentinel images at a five-year interval or modified according to user feedbacks. The updated glacial lake dataset will continue to be released freely and publicly on the Mountain Science Data Center sharing platform.

7 Data availability

Our glacial lake dataset extracted from Sentinel-2 images in 2020 and Landsat observation between 1990 and 2020 are available online via the Mountain Science Data Center, the Institute of Mountain Hazards and Environment, the Chinese Academy of Sciences at <https://doi.org/10.12380/Glaci.msdc.000001> (Lesi et al., 2022). The glacial lake dataset is provided in both ESRI shapefile format (total size of 22.6 MB) and the Geopackage format (version 1.2.1) with a total size of 9.2MB, which can be opened and further processed by open-source geographic information system software such as QGIS.

8 Conclusions

Glacial lake inventories of the entire China-Pakistan Economic Corridor in 2020 were provided based on Landsat and Sentinel-2 images using a threshold-based semi-automated mapping method. Both Landsat and Sentinel-2 derived glacial lake dataset show similar characteristics in spatial distribution and in the statistics of count and area. By contrast, glacial lake dataset derived from Sentinel-2 images with a spatial resolution of 10 m has a lower mapping error and more accurate lake boundary than those from 30 m spatial resolution Landsat images whereas Landsat imagery is more suitable to analyze spatial-temporal changes at a longer time scale due to its long-term archived observations at a consistent 30 m spatial resolution starting from the late 1980s.

Glacial lakes in the study area remain relatively stable with a slight increase in number and area between 1990 and 2020 according to Landsat observations. Our dataset reveals that 2154 glacial lakes in 1990 covering $85.1 \pm 14.66 \text{ km}^2$ increased to 2234 lakes with a total area of $86.31 \pm 14.98 \text{ km}^2$. The same mapping method and rigorous workflow of quality assurance and quality control used in this study reduced the error in multi-temporal changes of glacial lakes.

The Hanshaw's error estimation method for pixel-based lake mapping was improved by removing repeatedly calculated edge pixels that vary with lake shape. Therefore, the newly proposed method reduces the estimated value of uncertainty from satellite observations. The average relative error is $\pm 17.36\%$ for Landsat-derived product and $\pm 8.15\%$ for product from Sentinel-2.

Our glacial lake dataset contains a range of critical parameters that maximize their potential utility for water resource and GLOFs risk evaluation, cryosphere-hydrological and glacier-lake evolution projection. The dual classification systems of glacial lake types were developed and are very likely to attract broader researchers and scientists to use our datasets.

641 In comparison with other existing glacial lake datasets, our products were created through a
642 thorough consideration of lake types, cross checks and rigorous quality assurance, and will be
643 updated and released continuously in the Mountain Science Data Center. As such, we expect
644 that our glacial lake dataset will have significant value to cryospheric-hydrology research, the
645 assessment of water resource and glacier-related hazards in the CPEC.

646
647 **Appendix.** The appendix related to this article is available online.

648
649 **Author contributions.** ML and YN conceived the study, ML, YN and XD performed data
650 processing and analysis of the glacial lake inventory data, JW contributed to tool
651 development and mapping methods, ML and YN wrote the manuscript. All authors reviewed
652 and edited the manuscript before submission.

653
654 **Competing interests.** The authors declare no conflict of interest.

655
656 **Acknowledgements.**

657 We are grateful for the editor Kenneth Mankoff and three anonymous referees for their
658 constructive comments that greatly help us to improve this manuscript. This study was
659 supported by the second Tibetan Plateau Scientific Expedition and Research Program (grant
660 2019QZKK0603), the National Natural Science Foundation of China (Grant Nos. 42171086,
661 41971153), the International Science & Technology Cooperation Program of China (No.
662 2018YFE0100100), the Chinese Academy of Sciences “Light of West China” and Natural
663 Sciences and Engineering Research Council of Canada (Grant No. DG-2020-04207).

664
665

666 **Appendix**

667 **Tutorial for Improved Uncertainty Estimating Method**

668
669 The Hanshaw’s equation was originally proposed for pixelated polygons (such as a polygon
670 directly extracted from a remote sensing image), and performed more robustly than manually
671 digitized polygons (where vertices do not necessarily follow the pixel edges). Our improved
672 method also performs better for pixelated polygons. This tutorial is dedicated to helping
673 implement our improved uncertainty estimation method.

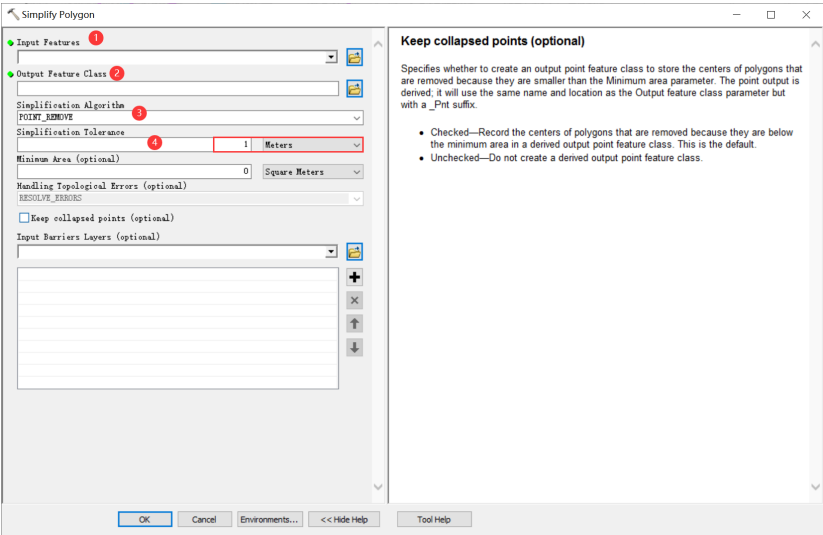
674
675 **Procedure of uncertainty estimating method (using ArcGIS (© ESRI) for example)**

676 1. Removing redundant nodes (optional)

677 We found that a small proportion (~1%) of the pixelated lake polygons (directly extracted
678 from satellite images) have redundant nodes, which affects the value of inner nodes. If no
679 redundant nodes exist, this step can be skipped. Or, we recommend using the “Simplify
680 Polygon” tool in ArcGIS to remove those nodes (Figure A1Figure A1).

- 681 In the Simplify Polygon panel
- 682 • Input your dataset.
- 683 • Set the output path and output file name.
- 684 • Choose the simplification algorithm. We recommended “POINT_REMOVE”.
- 685 • Set the tolerance of simplification algorithm. In this step, we need to ensure that the
- 686 polygon boundaries remain unchanged after deleting redundant nodes. Generally, a
- 687 tolerance of 1 meter will suffice, or you can adjust the threshold until your satisfaction.

带格式的: 字体: 非加粗



688
689 **Figure A1. Input and option for Simplify Polygon in ArcGIS.**
690

- 691 2. Calculating the total number of nodes using ArcGIS (Figure A2):
- 692 • Add a new field in the attribute table of dataset.
- 693 • Open Field Calculator.
- 694 • Switch the parser to python mode, and enter the following code “!shape.pointcount!” in
- 695 the blue box to calculate the total number of nodes for each glacial lake boundary.

带格式的: 字体: 非加粗

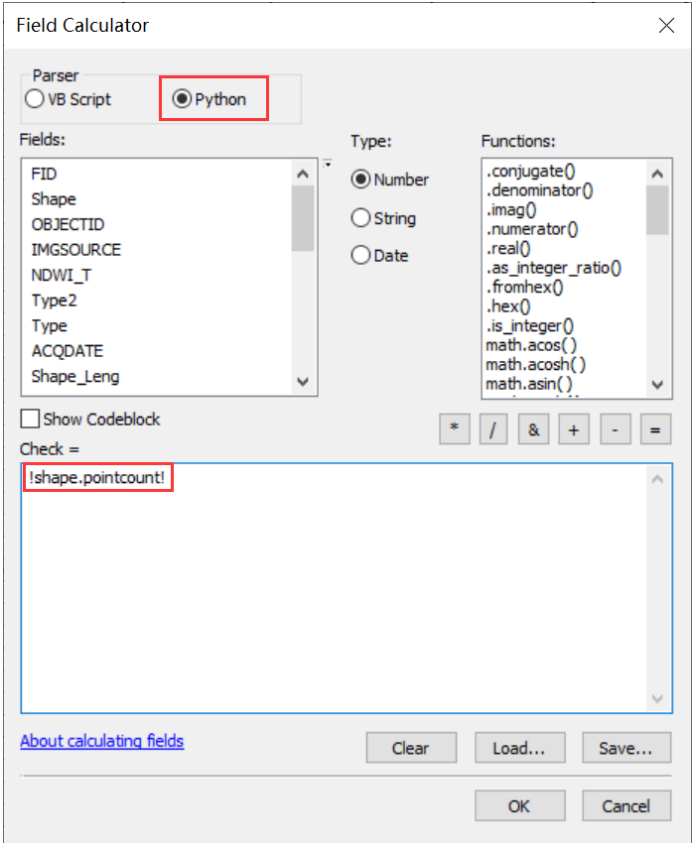


Figure A2. Total node calculation in ArcGIS.

- 699 3. Calculating the number of inner nodes:

701 For polygons without islands (Figure A3), use the equation 5. An inner node is a

702 polygon vertex where the interior angle surrounding it is greater than 180 degrees. An outer

703 node is the opposite of the inner node, where the interior angle is less than 180 degrees. We

704 found that the outer nodes are usually four more than the inner nodes in our glacial lake

705 dataset. The total nodes in ArcGIS contain one overlapping node to close the polygon,

706 meaning the endpoint is also the startpoint. This extra count was deleted in the calculation

707 (equation 5).

带格式的: 字体: 非加粗

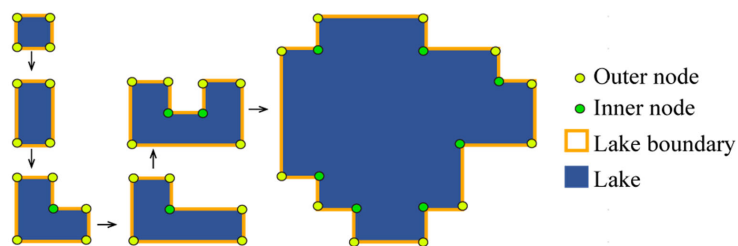


Figure A3. Sketch of outer and inner nodes of various glacial lakes without island.

For polygons with island (Figure A4) use the equation 6.

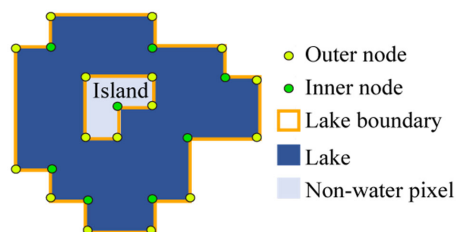


Figure A4. Sketch of outer and inner nodes for glacial lake with island.

We further specify the steps below to help implement equation 6.

Sept 1: detect the number of islands within each polygon.

- Convert the initial lake polygon to polyline using the “Feature To Line” tool (Figure A5).

带格式的: 字体: 非加粗

带格式的: 字体: 非加粗

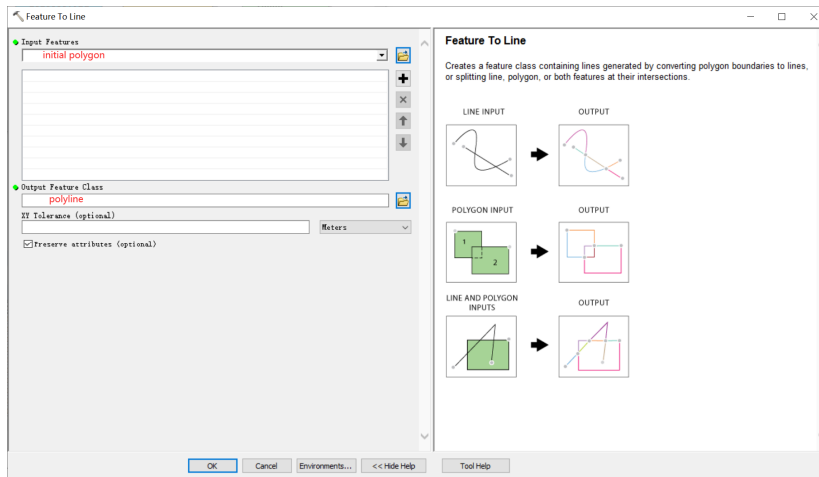


Figure A5. Feature To Line tool in ArcGIS

- Convert the polyline to generate a new polygon (Figure A6Figure A6).

带格式的: 字体: 非加粗

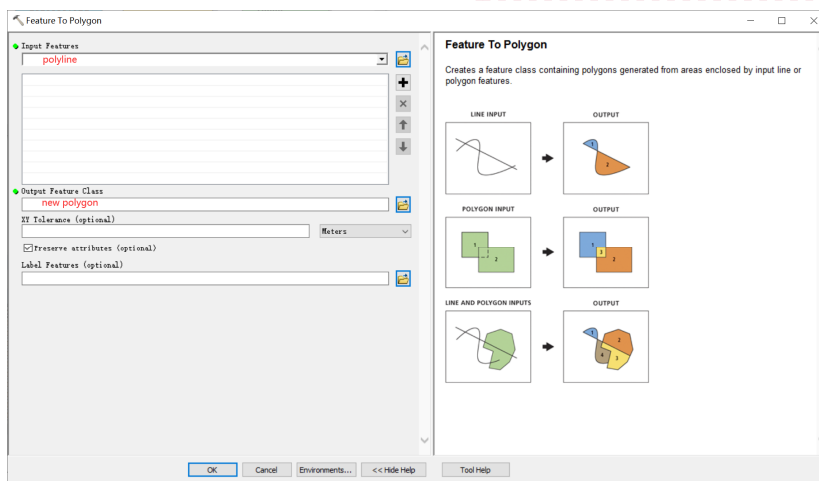


Figure A6. Feature To Polygon tool in ArcGIS

- Erase the new polygon by the initial polygon, which outputs the islands. Then we can count how many islands there are in each lake (Figure A7Figure A7).

带格式的: 字体: 非加粗

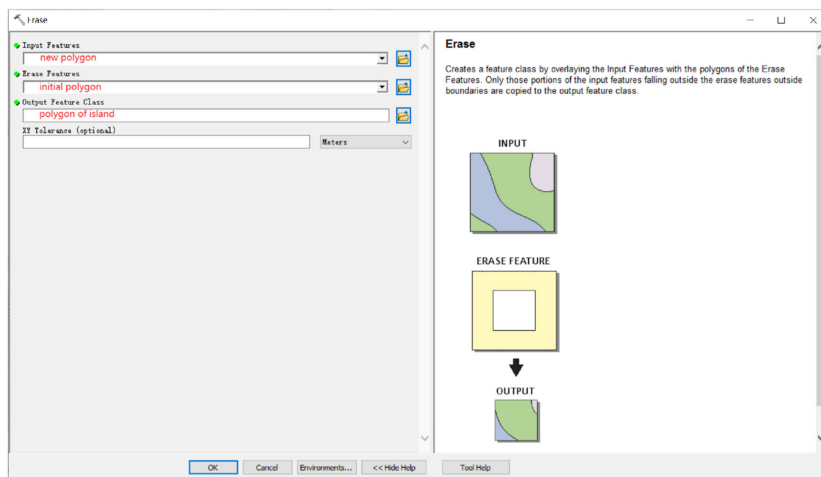


Figure A7. Erase tool in ArcGIS.

Step 2: calculate the number of inner nodes for each polygon with island using equation 6.

4. Calculating the uncertainty of lake mapping using equation 4.

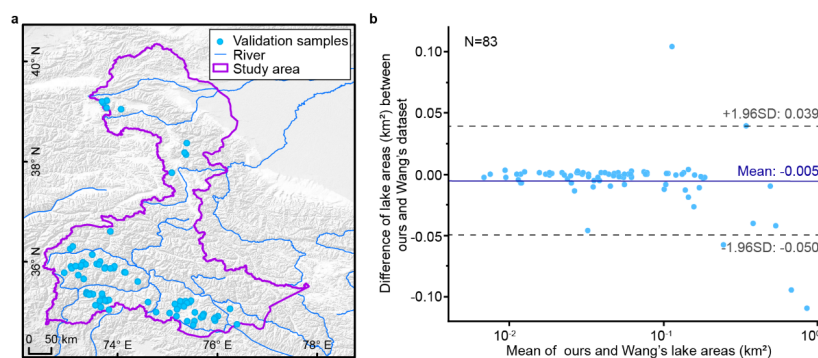


Figure A8. Distribution of validation samples (a) and comparison of glacial lakes (b) derived from our Landsat product in 2020 and Wang's lake data in 2018.

References

- Ashraf, A., Naz, R., Iqbal, M.B.: Altitudinal dynamics of glacial lakes under changing climate in the Hindu Kush, Karakoram, and Himalaya ranges. *Geomorphology*, 283: 72-79, <https://doi.org/10.1016/j.geomorph.2017.01.033>, 2017.

带格式的：与下段同页

带格式的：字体：加粗

带格式的：字体：(默认) Times New Roman, 加粗

带格式的：字体：加粗

带格式的：字体：(默认) Times New Roman

带格式的：题注，两端对齐，定义网格后自动调整右缩进，调整中文与西文文字的间距，调整中文与数字的间距

带格式的：字体：(中文) Times New Roman, 字体颜色：自动设置

746 Azam, M.F., Kargel, J.S., Shea, J.M., Nepal, S., Haritashya, U.K., Srivastava, S., Maussion, F., Qazi, N.,
 747 Chevallier, P., Dimri, A.P., Kulkarni, A.V., Cogley, J.G., Bahuguna, I.: Glaciohydrology of the Himalaya-
 748 Karakoram. *Science*, 373: eabf3668, <https://doi.org/10.1126/science.abf3668>, 2021.
 749 Battamo, A.Y., Varis, O., Sun, P., Yang, Y., Oba, B.T., Zhao, L.: Mapping socio-ecological resilience along the
 750 seven economic corridors of the Belt and Road Initiative. *J. Clean. Prod.*, 309: 127341,
 751 <https://doi.org/10.1016/j.jclepro.2021.127341>, 2021.
 752 Bhambri, R., Hewitt, K., Kawishwar, P., Kumar, A., Verma, A., Snehamani, Tiwari, S., Misra, A.: Ice-dams,
 753 outburst floods, and movement heterogeneity of glaciers, Karakoram. *Global Planet. Change*, 180: 100-116,
 754 <https://doi.org/10.1016/j.gloplacha.2019.05.004>, 2019.
 755 Bhattacharya, A., Bolch, T., Mukherjee, K., King, O., Menounos, B., Kapitsa, V., Neckel, N., Yang, W., Yao,
 756 T.: High Mountain Asian glacier response to climate revealed by multi-temporal satellite observations since the
 757 1960s. *Nat. Commun.*, 12: 4133, <https://doi.org/10.1038/s41467-021-24180-y>, 2021.
 758 Bolch, T., Pieczonka, T., Mukherjee, K., Shea, J.: Brief communication: Glaciers in the Hunza catchment
 759 (Karakoram) have been nearly in balance since the 1970s. *The Cryosphere*, 11: 531-539,
 760 <https://doi.org/10.5194/tc-11-531-2017>, 2017.
 761 Brun, F., Berthier, E., Wagnon, P., Kääb, A., Treichler, D.: A spatially resolved estimate of High Mountain Asia
 762 glacier mass balances from 2000 to 2016. *Nat. Geosci.*, 10: 668-673, <https://doi.org/10.1038/ngeo2999>, 2017.
 763 Brun, F., Wagnon, P., Berthier, E., Jomelli, V., Maharjan, S.B., Shrestha, F., Kraaijenbrink, P.D.A.:
 764 Heterogeneous Influence of Glacier Morphology on the Mass Balance Variability in High Mountain Asia.
 765 *Journal of Geophysical Research: Earth Surface*, 124: 1331-1345, <https://doi.org/10.1029/2018JF004838>, 2019.
 766 Carrivick, J.L., Tweed, F.S.: Proglacial lakes: character, behaviour and geological importance. *Quaternary Sci.*
 767 *Rev.*, 78: 34-52, <https://doi.org/10.1016/j.quascirev.2013.07.028>, 2013.

768 Carrivick, J.L., Quincey, D.J.: Progressive increase in number and volume of ice-marginal lakes on the western
769 margin of the Greenland Ice Sheet. *Global Planet. Change*, 116: 156-163,
770 <https://doi.org/10.1016/j.gloplacha.2014.02.009>, 2014.

771 Carrivick, J.L., Tweed, F.S.: A global assessment of the societal impacts of glacier outburst floods. *Global*
772 *Planet. Change*, 144: 1-16, <https://doi.org/10.1016/j.gloplacha.2016.07.001>, 2016.

773 Carrivick, J.L., Tweed, F.S., Sutherland, J.L., Mallalieu, J.: Toward Numerical Modeling of Interactions
774 Between Ice-Marginal Proglacial Lakes and Glaciers. *Frontiers in Earth Science*, 8,
775 <https://doi.org/10.3389/feart.2020.577068>, 2020.

776 Carrivick, J.L., How, P., Lea, J.M., Sutherland, J.L., Grimes, M., Tweed, F.S., Cornford, S., Quincey, D.J.,
777 Mallalieu, J.: Ice-Marginal Proglacial Lakes Across Greenland: Present Status and a Possible Future. *Geophys.*
778 *Res. Lett.*, 49: e2022GL099276, <https://doi.org/10.1029/2022GL099276>, 2022.

779 Chen, F., Zhang, M., Guo, H., Allen, S., Kargel, J.S., Haritashya, U.K., Watson, C.S.: Annual 30 m dataset for
780 glacial lakes in High Mountain Asia from 2008 to 2017. *Earth System Science Data*, 13: 741-766,
781 <https://doi.org/10.5194/essd-13-741-2021>, 2021.

782 Chen, X., Cui, P., You, Y., Cheng, Z., Khan, A., Ye, C., Zhang, S.: Dam-break risk analysis of the Attabad
783 landslide dam in Pakistan and emergency countermeasures. *Landslides*, 14: 675-683,
784 <https://doi.org/10.1007/s10346-016-0721-7>, 2017.

785 Cook, S.J., Quincey, D.J.: Estimating the volume of Alpine glacial lakes. *Earth Surf. Dynam.*, 3: 559-575,
786 <https://doi.org/10.5194/esurf-3-559-2015>, 2015.

787 Emmer, A., Cuřín, V.: Can a dam type of an alpine lake be derived from lake geometry? A negative result. *J.*
788 *Mt. Sci.-Engl.*, 18: 614-621, <https://doi.org/10.1007/s11629-020-6003-9>, 2021.

789 Farr, T.G., Rosen, P.A., Caro, E., Crippen, R., Duren, R., Hensley, S., Kobrick, M., Paller, M., Rodriguez, E.,
790 Roth, L., Seal, D., Shaffer, S., Shimada, J., Umland, J., Werner, M., Oskin, M., Burbank, D., Alsdorf, D.: The
791 Shuttle Radar Topography Mission. *Rev. Geophys.*, 45: RG2004, <https://doi.org/10.1029/2005RG000183>, 2007.
792 Gardelle, J., Arnaud, Y., Berthier, E.: Contrasted evolution of glacial lakes along the Hindu Kush Himalaya
793 mountain range between 1990 and 2009. *Global Planet. Change*, 75: 47-55,
794 <https://doi.org/10.1016/j.gloplacha.2010.10.003>, 2011.
795 Hanshaw, M.N., Bookhagen, B.: Glacial areas, lake areas, and snow lines from 1975 to 2012: status of the
796 Cordillera Vilcanota, including the Quelccaya Ice Cap, northern central Andes, Peru. *The Cryosphere*, 8: 359-
797 376, <https://doi.org/10.5194/tc-8-359-2014>, 2014.
798 Hewitt, K.: The Karakoram Anomaly? Glacier Expansion and the 'Elevation Effect,' Karakoram Himalaya. *Mt.*
799 *Res. Dev.*, 25: 332-340, [https://doi.org/10.1659/0276-4741\(2005\)025\[0332:TKAGEA\]2.0.CO;2](https://doi.org/10.1659/0276-4741(2005)025[0332:TKAGEA]2.0.CO;2), 2005.
800 Hewitt, K., 2014. *Glaciers of the Karakoram Himalaya: Glacial Environments, Processes, Hazards and*
801 *Resources*. Springer, Dordrecht.
802 How, P., Messerli, A., Mätzler, E., Santoro, M., Wiesmann, A., Caduff, R., Langley, K., Bojesen, M.H., Paul,
803 F., Kääb, A., Carrivick, J.L.: Greenland-wide inventory of ice marginal lakes using a multi-method approach.
804 *Sci. Rep.-UK*, 11: 4481, <https://doi.org/10.1038/s41598-021-83509-1>, 2021.
805 Huggel, C., Kääb, A., Haeberli, W., Teyssie, P., Paul, F.: Remote sensing based assessment of hazards from
806 glacier lake outbursts: a case study in the Swiss Alps. *Can. Geotech. J.*, 39: 316-330,
807 <https://doi.org/10.1139/t01-099>, 2002.
808 Hugonnet, R., McNabb, R., Berthier, E., Menounos, B., Nuth, C., Girod, L., Farinotti, D., Huss, M., Dussailant,
809 I., Brun, F., Kääb, A.: Accelerated global glacier mass loss in the early twenty-first century. *Nature*, 592: 726-
810 731, <https://doi.org/10.1038/s41586-021-03436-z>, 2021.

811 Huss, M., Hock, R.: Global-scale hydrological response to future glacier mass loss. *Nat. Clim. Change*, 8: 135-
812 140, <https://doi.org/10.1038/s41558-017-0049-x>, 2018.

813 Immerzeel, W.W., Lutz, A.F., Andrade, M., Bahl, A., Biemans, H., Bolch, T., Hyde, S., Brumby, S., Davies,
814 B.J., Elmore, A.C., Emmer, A., Feng, M., Fernández, A., Haritashya, U., Kargel, J.S., Koppes, M.,
815 Kraaijenbrink, P.D.A., Kulkarni, A.V., Mayewski, P.A., Nepal, S., Pacheco, P., Painter, T.H., Pellicciotti, F.,
816 Rajaram, H., Rupper, S., Sinisalo, A., Shrestha, A.B., Viviroli, D., Wada, Y., Xiao, C., Yao, T., Baillie, J.E.M.:
817 Importance and vulnerability of the world's water towers. *Nature*, 577: 364-369, [https://doi.org/10.1038/s41586-](https://doi.org/10.1038/s41586-019-1822-y)
818 019-1822-y, 2020.

819 Jarvis, A., Reuter, H.I., Nelson, A., Guevara, E., 2008. Hole-filled seamless SRTM data V4. 2008, International
820 Centre for Tropical Agriculture (CIAT), available from <http://srtm.csi.cgiar.org>.

821 Jiang, S., Nie, Y., Liu, Q., Wang, J., Liu, L., Hassan, J., Liu, X., Xu, X.: Glacier Change, Supraglacial Debris
822 Expansion and Glacial Lake Evolution in the Gyirong River Basin, Central Himalayas, between 1988 and 2015.
823 *Remote Sens.-Basel*, 10: 986, <https://doi.org/10.3390/rs10070986>, 2018.

824 Kääb, A., Berthier, E., Nuth, C., Gardelle, J., Arnaud, Y.: Contrasting patterns of early twenty-first-century
825 glacier mass change in the Himalayas. *Nature*, 488: 495-498, <https://doi.org/10.1038/nature11324>, 2012.

826 Lesi, M., Nie, Y., Shugar, D.H., Wang, J., Deng, Q., Chen, H.: Landsat and Sentinel-derived glacial lake dataset
827 in the China-Pakistan Economic Corridor from 1990 to 2020. Mountain Science Data Center,
828 <https://doi.org/10.12380/Glaci.msdc.000001> CSTR:1a006.11.Glaci.msdc.000001, 2022.

829 Li, D., Shangguan, D., Anjum, M.N.: Glacial Lake Inventory Derived from Landsat 8 OLI in 2016–2018 in
830 China–Pakistan Economic Corridor. *ISPRS international journal of geo-information*, 9: 294,
831 <https://doi.org/10.3390/ijgi9050294>, 2020.

832 Li, Z., Deng, X., Zhang, Y.: Evaluation and convergence analysis of socio-economic vulnerability to natural
833 hazards of Belt and Road Initiative countries. *J. Clean. Prod.*, 282: 125406,
834 <https://doi.org/10.1016/j.jclepro.2020.125406>, 2021.

835 Liu, Q., Mayer, C.: Distribution and interannual variability of supraglacial lakes on debris-covered glaciers in
836 the Khan Tengri-Tumor Mountains, Central Asia. *Environ. Res. Lett.*, 10: 014014 2015.

837 Liu, Q., Mayer, C., Wang, X., Nie, Y., Wu, K., Wei, J., Liu, S.: Interannual flow dynamics driven by frontal
838 retreat of a lake-terminating glacier in the Chinese Central Himalaya. *Earth Planet. Sc. Lett.*, 546: 116450,
839 <https://doi.org/10.1016/j.epsl.2020.116450>, 2020.

840 Lyons, E.A., Sheng, Y., Smith, L.C., Li, J., Hinkel, K.M., Lenters, J.D., Wang, J.: Quantifying sources of error
841 in multitemporal multisensor lake mapping. *Int. J. Remote Sens.*, 34: 7887-7905,
842 <https://doi.org/10.1080/01431161.2013.827343>, 2013.

843 Martín, C.N.S., Ponce, J.F., Montes, A., Balocchi, L.D., Gorza, C., Andrea, C.: Proglacial landform assemblage
844 in a rapidly retreating cirque glacier due to temperature increase since 1970, Fuegian Andes, Argentina.
845 *Geomorphology*, 390: 107861, <https://doi.org/10.1016/j.geomorph.2021.107861>, 2021.

846 Maurer, J.M., Schaefer, J.M., Rupper, S., Corley, A.: Acceleration of ice loss across the Himalayas over the past
847 40 years. *Science Advances*, 5: eaav7266, <https://doi.org/10.1126/sciadv.aav7266>, 2019.

848 Mcfeeters, S.K.: The use of the Normalized Difference Water Index (NDWI) in the delineation of open water
849 features. *Int. J. Remote Sens.*, 17: 1425 - 1432 1996.

850 Miles, E.S., Watson, C.S., Brun, F., Berthier, E., Esteves, M., Quincey, D.J., Miles, K.E., Hubbard, B., Wagnon,
851 P.: Glacial and geomorphic effects of a supraglacial lake drainage and outburst event, Everest region, Nepal
852 Himalaya. *The Cryosphere*, 12: 3891-3905, <https://doi.org/10.5194/tc-12-3891-2018>, 2018.

853 Nie, Y., Zhang, Y., Liu, L., Zhang, J.: Glacial change in the vicinity of Mt. Qomolangma (Everest), central high
 854 Himalayas since 1976. *J. Geogr. Sci.*, 20: 667-686, <https://doi.org/10.1007/s11442-010-0803-8>, 2010.
 855 Nie, Y., Sheng, Y., Liu, Q., Liu, L., Liu, S., Zhang, Y., Song, C.: A regional-scale assessment of Himalayan
 856 glacial lake changes using satellite observations from 1990 to 2015. *Remote Sens. Environ.*, 189: 1-13,
 857 <https://doi.org/10.1016/j.rse.2016.11.008>, 2017.
 858 Nie, Y., Liu, Q., Wang, J., Zhang, Y., Sheng, Y., Liu, S.: An inventory of historical glacial lake outburst floods
 859 in the Himalayas based on remote sensing observations and geomorphological analysis. *Geomorphology*, 308:
 860 91-106, <https://doi.org/10.1016/j.geomorph.2018.02.002>, 2018.
 861 Nie, Y., Liu, W., Liu, Q., Hu, X., Westoby, M.J.: Reconstructing the Chongbaxia Tsho glacial lake outburst
 862 flood in the Eastern Himalaya: Evolution, process and impacts. *Geomorphology*, 370: 107393,
 863 <https://doi.org/10.1016/j.geomorph.2020.107393>, 2020.
 864 Nie, Y., Pritchard, H.D., Liu, Q., Hennig, T., Wang, W., Wang, X., Liu, S., Nepal, S., Samyn, D., Hewitt, K.,
 865 Chen, X.: Glacial change and hydrological implications in the Himalaya and Karakoram. *Nature Reviews Earth*
 866 & Environment, 2: 91-106, <https://doi.org/10.1038/s43017-020-00124-w>, 2021.
 867 Paul, F., Rastner, P., Azzoni, R.S., Diolaiuti, G., Fugazza, D., Le Bris, R., Nemec, J., Rabatel, A., Ramusovic,
 868 M., Schwaizer, G., Smiraglia, C.: Glacier shrinkage in the Alps continues unabated as revealed by a new glacier
 869 inventory from Sentinel-2. *Earth System Science Data*, 12: 1805-1821, [https://doi.org/10.5194/essd-12-1805-](https://doi.org/10.5194/essd-12-1805-2020)
 870 2020, 2020.
 871 Pfeffer, W.T., Arendt, A.A., Bliss, A., Bolch, T., Cogley, J.G., Gardner, A.S., Hagen, J., Hock, R., Kaser, G.,
 872 Kienholz, C., Miles, E.S., Moholdt, G., Mölg, N., Paul, F., Radić, V., Rastner, P., Raup, B.H., Rich, J., Sharp,
 873 M.J.: The Randolph Glacier Inventory: a globally complete inventory of glaciers. *J. Glaciol.*, 60: 537-552,
 874 <https://doi.org/10.3189/2014JoG13J176>, 2014.

875 Post, A., Mayo, L.R., 1971. Glacier dammed lakes and outburst floods in Alaska: U.S. Geological Survey
876 Hydrologic Investigations Atlas 455, U.S. Geological Survey.

877 Pritchard, H.D.: Asia's shrinking glaciers protect large populations from drought stress. *Nature*, 569: 649-654,
878 <https://doi.org/10.1038/s41586-019-1240-1>, 2019.

879 Quincey, D.J., Richardson, S.D., Luckman, A., Lucas, R.M., Reynolds, J.M., Hambrey, M.J., Glasser, N.F.:
880 Early recognition of glacial lake hazards in the Himalaya using remote sensing datasets. *Global Planet. Change*,
881 56: 137-152, <https://doi.org/10.1016/j.gloplacha.2006.07.013>, 2007.

882 Rabus, B., Eineder, M., Roth, A., Bamler, R.: The shuttle radar topography mission—a new class of digital
883 elevation models acquired by spaceborne radar. *ISPRS J. Photogramm.*, 57: 241-262,
884 [https://doi.org/10.1016/S0924-2716\(02\)00124-7](https://doi.org/10.1016/S0924-2716(02)00124-7), 2003.

885 RGI Consortium: Randolph Glacier Inventory – A Dataset of Global Glacier Outlines: Version 6.0: Technical
886 Report, <https://doi.org/10.7265/N5-RGI-60>, 2017.

887 Rick, B., Mcgrath, D., Armstrong, W., McCoy, S.W.: Dam type and lake location characterize ice-marginal lake
888 area change in Alaska and NW Canada between 1984 and 2019. *The Cryosphere*, 16: 297-314,
889 <https://doi.org/10.5194/tc-16-297-2022>, 2022.

890 Rose, A., Mckee, J., Sims, K., Bright, E., Reith, A., Urban, M.: LandScan Global 2020,
891 <https://doi.org/https://doi.org/10.48690/1523378>, 2021.

892 Rounce, D.R., Hock, R., Shean, D.E.: Glacier Mass Change in High Mountain Asia Through 2100 Using the
893 Open-Source Python Glacier Evolution Model (PyGEM). *Frontiers in Earth Science*, 7: 331,
894 <https://doi.org/10.3389/feart.2019.00331>, 2020.

895 Roy, D.P., Wulder, M.A., Loveland, T.R., C. E., W., Allen, R.G., Anderson, M.C., Helder, D., Irons, J.R.,
896 Johnson, D.M., Kennedy, R., Scambos, T.A., Schaaf, C.B., Schott, J.R., Sheng, Y., Vermote, E.F., Belward,

897 A.S., Bindschadler, R., Cohen, W.B., Gao, F., Hipple, J.D., Hostert, P., Huntington, J., Justice, C.O., Kilic, A.,
898 Kovalskyy, V., Lee, Z.P., Lymburner, L., Masek, J.G., Mccorkel, J., Shuai, Y., Trezza, R., Vogelmann, J.,
899 Wynne, R.H., Zhu, Z.: Landsat-8: Science and product vision for terrestrial global change research. *Remote*
900 *Sens. Environ.*, 145: 154-172, <https://doi.org/10.1016/j.rse.2014.02.001>, 2014.

901 Sakai, A.: Brief communication: Updated GAMDAM glacier inventory over high-mountain Asia. *The*
902 *Cryosphere*, 13: 2043-2049, <https://doi.org/10.5194/tc-13-2043-2019>, 2019.

903 Salerno, F., Thakuri, S., D'Agata, C., Smiraglia, C., Manfredi, E.C., Viviano, G., Tartari, G.: Glacial lake
904 distribution in the Mount Everest region: Uncertainty of measurement and conditions of formation. *Global*
905 *Planet. Change*, 92-93: 30-39 2012.

906 Shean, D.E., Bhushan, S., Montesano, P., Rounce, D.R., Arendt, A., Osmanoglu, B.: A Systematic, Regional
907 Assessment of High Mountain Asia Glacier Mass Balance. *Frontiers in Earth Science*, 7: 363,
908 <https://doi.org/10.3389/feart.2019.00363>, 2020.

909 Sheng, Y., Song, C., Wang, J., Lyons, E.A., Knox, B.R., Cox, J.S., Gao, F.: Representative lake water extent
910 mapping at continental scales using multi-temporal Landsat-8 imagery. *Remote Sens. Environ.*, 185: 129-141,
911 <https://doi.org/10.1016/j.rse.2015.12.041>, 2016.

912 Shugar, D.H., Burr, A., Haritashya, U.K., Kargel, J.S., Watson, C.S., Kennedy, M.C., Bevington, A.R., Betts,
913 R.A., Harrison, S., Stratman, K.: Rapid worldwide growth of glacial lakes since 1990. *Nat. Clim. Change*, 10:
914 939-945, <https://doi.org/10.1038/s41558-020-0855-4>, 2020.

915 Shugar, D.H., Jacquemart, M., Shean, D., Bhushan, S., Upadhyay, K., Sattar, A., Schwanghart, W., McBride, S.,
916 de Vries, M., Mergili, M., Emmer, A., Deschamps-Berger, C., McDonnell, M., Bhambri, R., Allen, S., Berthier,
917 E., Carrivick, J.L., Clague, J.J., Dokukin, M., Dunning, S.A., Frey, H., Gascoin, S., Haritashya, U.K., Huggel,
918 C., Kaab, A., Kargel, J.S., Kavanaugh, J.L., Lacroix, P., Petley, D., Rupper, S., Azam, M.F., Cook, S.J., Dimri,

919 A.P., Eriksson, M., Farinotti, D., Fiddes, J., Gnyawali, K.R., Harrison, S., Jha, M., Koppes, M., Kumar, A.,
920 Leinss, S., Majeed, U., Mal, S., Muhuri, A., Noetzli, J., Paul, F., Rashid, I., Sain, K., Steiner, J., Ugalde, F.,
921 Watson, C.S., Westoby, M.J.: A massive rock and ice avalanche caused the 2021 disaster at Chamoli, Indian
922 Himalaya. *Science*, 373: 300-306, <https://doi.org/10.1126/science.abh4455>, 2021.

923 Ullah, S., You, Q., Ali, A., Ullah, W., Jan, M.A., Zhang, Y., Xie, W., Xie, X.: Observed changes in maximum
924 and minimum temperatures over China- Pakistan economic corridor during 1980–2016. *Atmos. Res.*, 216: 37-
925 51, <https://doi.org/10.1016/j.atmosres.2018.09.020>, 2019.

926 Viviroli, D., Kumm, M., Meybeck, M., Kallio, M., Wada, Y.: Increasing dependence of lowland populations
927 on mountain water resources. *Nature Sustainability*, 3: 917-928, <https://doi.org/10.1038/s41893-020-0559-9>,
928 2020.

929 Wang, J., Sheng, Y., Tong, T.S.D.: Monitoring decadal lake dynamics across the Yangtze Basin downstream of
930 Three Gorges Dam. *Remote Sens. Environ.*, 152: 251-269, <https://doi.org/10.1016/j.rse.2014.06.004>, 2014.

931 Wang, J., Sheng, Y., Wada, Y.: Little impact of the Three Gorges Dam on recent decadal lake decline across
932 China's Yangtze Plain. *Water Resour. Res.*, 53: 3854-3877, <https://doi.org/10.1002/2016WR019817>, 2017.

933 Wang, J., Song, C., Reager, J.T., Yao, F., Famiglietti, J.S., Sheng, Y., Macdonald, G.M., Brun, F., Schmied,
934 H.M., Marston, R.A., Wada, Y.: Recent global decline in endorheic basin water storages. *Nat. Geosci.*, 11: 926-
935 932, <https://doi.org/10.1038/s41561-018-0265-7>, 2018.

936 Wang, X., Ding, Y., Liu, S., Jiang, L., Wu, K., Jiang, Z., Guo, W.: Changes of glacial lakes and implications in
937 Tian Shan, Central Asia, based on remote sensing data from 1990 to 2010. *Environ. Res. Lett.*, 8: 44052,
938 <https://doi.org/10.1088/1748-9326/8/4/044052>, 2013.

939 Wang, X., Liu, S., Zhang, J.: A new look at roles of the cryosphere in sustainable development. *Advances in*
940 *Climate Change Research*, 10: 124-131, <https://doi.org/10.1016/j.accre.2019.06.005>, 2019.

941 Wang, X., Guo, X., Yang, C., Liu, Q., Wei, J., Zhang, Y., Liu, S., Zhang, Y., Jiang, Z., Tang, Z.: Glacial lake
 942 inventory of high-mountain Asia in 1990 and 2018 derived from Landsat images. *Earth System Science Data*,
 943 12: 2169-2182, <https://doi.org/10.5194/essd-12-2169-2020>, 2020.
 944 Wangchuk, S., Bolch, T.: Mapping of glacial lakes using Sentinel-1 and Sentinel-2 data and a random forest
 945 classifier: Strengths and challenges. *Science of Remote Sensing*, 2: 100008,
 946 <https://doi.org/https://doi.org/10.1016/j.srs.2020.100008>, 2020.
 947 Westoby, M.J., Glasser, N.F., Brasington, J., Hambrey, M.J., Quincey, D.J., Reynolds, J.M.: Modelling outburst
 948 floods from moraine-dammed glacial lakes. *Earth-Sci. Rev.*, 134: 137-159,
 949 <https://doi.org/10.1016/j.earscirev.2014.03.009>, 2014.
 950 Williamson, A.G., Banwell, A.F., Willis, I.C., Arnold, N.S.: Dual-satellite (Sentinel-2 and Landsat 8) remote
 951 sensing of supraglacial lakes in Greenland. *The Cryosphere*, 12: 3045-3065, [https://doi.org/10.5194/tc-12-3045-](https://doi.org/10.5194/tc-12-3045-2018)
 952 2018, 2018.
 953 Wu, R., Liu, G., Zhang, R., Wang, X., Li, Y., Zhang, B., Cai, J., Xiang, W.: A Deep Learning Method for
 954 Mapping Glacial Lakes from the Combined Use of Synthetic-Aperture Radar and Optical Satellite Images.
 955 *Remote Sens.-Basel*, 12: 4020
 956 2020.
 957 Wulder, M.A., Loveland, T.R., Roy, D.P., Crawford, C.J., Masek, J.G., Woodcock, C.E., Allen, R.G.,
 958 Anderson, M.C., Belward, A.S., Cohen, W.B., Dwyer, J., Erb, A., Gao, F., Griffiths, P., Helder, D., Hermosilla,
 959 T., Hipple, J.D., Hostert, P., Hughes, M.J., Huntington, J., Johnson, D.M., Kennedy, R., Kilic, A., Li, Z.,
 960 Lymburner, L., Mccorkel, J., Pahlevan, N., Scambos, T.A., Schaaf, C., Schott, J.R., Sheng, Y., Storey, J.,
 961 Vermote, E., Vogelmann, J., White, J.C., Wynne, R.H., Zhu, Z.: Current status of Landsat program, science, and

962 applications. *Remote Sens. Environ.*, 225: 127-147, <https://doi.org/https://doi.org/10.1016/j.rse.2019.02.015>,
 963 2019.
 964 Yao, C., Wang, X., Zhao, X., Wei, J., Zhang, Y.: Temporal and Spatial Changes of Glacial Lakes in the China-
 965 Pakistan Economic Corridor from 1990 to 2018. *Journal of Glaciology and Geocryology*, 42: 33-42,
 966 <https://doi.org/https://doi.org/10.7522/j.issn.1000-0240.2020.0009>, 2020.
 967 Yao, T., Thompson, L., Yang, W., Yu, W.S., Gao, Y., Guo, X.J., Yang, X.X., Duan, K.Q., Zhao, H.B., Xu,
 968 B.Q., Pu, J.C., Lu, A.X., Xiang, Y., Kattel, D.B., Joswiak, D.: Different glacier status with atmospheric
 969 circulations in Tibetan Plateau and surroundings. *Nat. Clim. Change*, 2: 663-667,
 970 <https://doi.org/10.1038/NCLIMATE1580>, 2012.
 971 Yao, X., Liu, S., Han, L., Sun, M., Zhao, L.: Definition and classification system of glacial lake for inventory
 972 and hazards study. *J. Geogr. Sci.*, 28: 193-205, <https://doi.org/10.1007/s11442-018-1467-z>, 2018.
 973 Zhang, G., Yao, T., Xie, H., Wang, W., Yang, W.: An inventory of glacial lakes in the Third Pole region and
 974 their changes in response to global warming. *Global Planet. Change*, 131: 148-157,
 975 <https://doi.org/10.1016/j.gloplacha.2015.05.013>, 2015.
 976 Zhang, M., Chen, F., Tian, B.: An automated method for glacial lake mapping in High Mountain Asia using
 977 Landsat 8 imagery. *J. Mt. Sci.-Engl.*, 15: 13-24, <https://doi.org/10.1007/s11629-017-4518-5>, 2018.
 978 Zhao, W., Xiong, D., Wen, F., Wang, X.: Lake area monitoring based on land surface temperature in the Tibetan
 979 Plateau from 2000 to 2018. *Environ. Res. Lett.*, 15, <https://doi.org/10.1088/1748-9326/ab9b41>, 2020.
 980 Zheng, G., Allen, S.K., Bao, A., Ballesteros-Cánovas, J.A., Huss, M., Zhang, G., Li, J., Yuan, Y., Jiang, L., Yu,
 981 T., Chen, W., Stoffel, M.: Increasing risk of glacial lake outburst floods from future Third Pole deglaciation.
 982 *Nat. Clim. Change*, 11: 411-417, <https://doi.org/10.1038/s41558-021-01028-3>, 2021.
 983